SEMMELWEIS EGYETEM

DOKTORI ISKOLA

Ph.D. értekezések

3231.

KOVÁCS SZONJA ANNA

Molekuláris és experimentális onkológia

című program

Programvezető: Dr. Bödör Csaba, egyetemi tanár

Témavezető: Dr. Győrffy Balázs, egyetemi tanár

INVESTIGATION OF IMMUNE CHECKPOINT INHIBITOR BIOMARKERS IN SOLID TUMORS

PhD thesis

Szonja Anna Kovács

Semmelweis University Doctoral School

Pathological and Oncological Division

Supervisor: Balázs Győrffy, MD, D.Sc.

Official reviewers: Kornélia Baghy, Ph.D.
Gabriella Emri, MD, Ph.D.

Head of the Complex Examination Committee: Sarolta Kárpáti, MD, D.Sc.

Members of the Complex Examination Committee: Dániel Veres, MD, Ph.D.
András Füredi, Ph.D.

Budapest
2025

TABLE OF CONTENTS

LIST OF ABBREVATIONS

AKT: AKT serine/threonine kinase

AQP1: aquaporin 1

ATCC: American Type Culture Collection

AUC: area under the curve

BCL2: BCL2 apoptosis regulator

BCORL1: BCL6 corepressor like 1

BLCAP: bladder cancer-associated protein

BRAF: B-Raf proto-oncogene, serine/threonine kinase

CDCA4: cell division cycle associated 4

CTLA-4: cytotoxic T lymphocyte-associated protein 4

DAB: diaminobenzidine

DDX10: DEAD-box helicase 10

DEK: DEK Proto-Oncogene

DMEM: Dulbecco's Modified Eagle's Medium

DMSO: dimethyl sulfoxide

FBS: fetal bovine serum

FDA: United States Food and Drug Administration

FGFR: fibroblast growth factor receptor

HLA-A: human leukocyte antigen A

HR: hazard ratio

HRP: horseradish peroxidase

HSPA1B: heat shock protein family A (Hsp70) member 1B

H&E: hematoxylin and eosin

ICI: immune checkpoint inhibitor

IDO1: indoleamine 2,3-dioxygenase-1

JAK: Janus kinase

KIT: KIT proto-oncogene, receptor tyrosine kinase

LAG-3: lymphocyte-activation gene 3

MAPK: mitogen-activated kinase kinase

MAP4K: mitogen-activated kinase kinase kinase kinase

MOB1A/B: MOB kinase activator 1A/B

NF1: neurofibromin 1

NRAS: NRAS proto-oncogene, GTPase

MSI-H/dMMR: microsatellite instability-high/mismatch repair deficient

PBS: phosphate buffered saline

PD-1: programmed cell death 1

PD-L1: programmed cell death ligand 1

PI3K: phosphoinositide 3-kinase

PRISMA: Preferred Reporting Items for Systematic reviews and Meta-Analyses

PRKC: protein kinase C

PTBP1: polypyrimidine tract binding protein 1

PTEN: phosphatase and tensin homolog

RAF-1: Raf-1 proto-oncogene, serine/threonine kinase

RLU: relative luminescence unit

ROC: receiver operating characteristic

ROS1: c-ros oncogene 1, receptor tyrosine kinase

RT-qPCR: quantitative reverse transcription polymerase chain reaction

SAV1: salvador family WW domain containing protein 1

SETD7: SET domain containing 7

SOX4: SRY-box transcription factor 4

SRC: SRC proto-oncogene, non-receptor tyrosine kinase

STAT: signal transducer and activator of transcription

STK35: serine/threonine kinase 35

TIGIT: T cell immunoreceptor with immunoglobulin and ITIM domain

TIM-3: T-cell immunoglobulin and mucin-domain containing-3

VISTA: V domain immunoglobulin suppressor of T cell activation

VP: verteporfin

WWTR1: WW domain containing transcription regulator 1

YAP1: yes-associated protein 1

1. INTRODUCTION

1.1. Cancer progression

Cancer remains as the second leading cause of death. Cancer incidence has been gradually declining amongst men but remained constant since 2011 (1). However, incidence in women has risen 23% since 1978 – according to the National Cancer Institute's (NCI's) Surveillance, Epidemiology, and End Results (SEER) by American Cancer Society (1). However, 5-year survival increased to 69% of all cancers combined in the 2010's, and mortality dropped by 34% since the 1990's (1). These data may look promising – yet cancer is still a public health issue.

The Cancer Genome Atlas (TCGA) has now provided an almost complete registry of cancer driver genes (2). However, these mutated genes are also widely found in normal tissues, indicating that their presence alone is not enough to trigger tumor formation (3). Malignant transformation results from the complex interplay of genetic alterations (including single nucleotide variants, mutations, copy number changes, and chromosomal abnormalities), epigenetic modifications (shifts in DNA methylation-acetylation balance, dysfunctional chromatin topology, and epitranscriptome changes), and environmental factors (including chronic inflammation, chemical and oxidative stress, metabolic factors; diet, microbiome composition; viral or bacterial infections, and aging) (4). Several pathways are involved in cancer progression, as summarized by the Hallmarks of Cancer: sustaining proliferative signalling, evading growth suppressors, resisting cell death, enabling replicative immortality, inducing or accessing vasculature, activating invasion and metastasis, reprogramming cellular metabolism, and avoiding immune destruction (5).

1.2. Immune checkpoint inhibitors

Under physiological conditions, immune checkpoints play a vital role in preventing excessive inflammation, and act as "brakes" to protect against autoimmunity. However, cancer cells can exploit these checkpoints to suppress immune responses, allowing them to avoid detection and destruction by T-cell-mediated immune responses, both innate (via $CD8^+$ cytotoxic T cells) and adaptive (via $CD4^+$ helper T cells) (6).

Cytotoxic T lymphocyte-associated protein 4 (CTLA-4, also known as CD152) was the first immune checkpoint targeted in clinical therapy as ipilimumab was accepted

in 2011 for the treatment of metastatic melanoma (7). Since then, the United States Food and Drug Administration (FDA) granted approval for the treatment of advanced renal cell carcinoma (8,9), microsatellite instability-high/mismatch repair deficient (MSI-H/dMMR) metastatic colorectal carcinoma (10), hepatocellular carcinoma (11), advanced/ metastatic non-small cell lung cancer (NSCLC) or extensive-stage small cell lung cancer (12,13), and for unresectable malignant pleural mesothelioma (14). Tremelimumab anti-CTLA-4 monoclonal antibody (mAb) received an Orphan Drug Designation for malignant mesothelioma by the FDA for unresectable hepatocellular carcinoma and NSCLC as a combination therapy (15,16). CTLA-4 competes with CD28, a positive costimulatory receptor on T cells, for the recognition of ligands CD80 (B7-1) and CD86 (B7-2) (16). Upon binding, CTLA-4 delivers inhibitory signals, preventing $CD4^+$ T cell activation,- proliferation,- trafficking, and IL-2 production (16).

Another critical immune checkpoint is the programmed cell death 1 (PD-1) receptor, which is expressed on a wide range of immune cells, and regulates T cell activation and tolerance, ultimately reducing inflammation (17). It has two ligands: programmed cell death ligand 1 (PD-L1, also called CD274) and programmed cell death ligand 2 (PD-L2, also called CD273) (17). PD-L1 is expressed on somatic and hematopoietic cells, but can be upregulated in tumor and stromal cells, too – such as on exhausted $CD8^+$ T cells. PD-L2 is primarily found on dendritic cells, macrophages, and mast cells, but also on tumor and stromal cells (18). Their interaction with PD-1 contributes to T cell exhaustion, immunosuppression, the induction of regulatory T cells (Tregs), and diminished cytotoxic T cell activity (17). Pembrolizumab was the first PD-1-targeting mAb approved by the FDA for unresectable or metastatic melanoma (19) and NSCLC (20). Since then, pembrolizumab has been approved for most solid tumors (triple-negative breast cancer (21), cervical cancer (22), urothelial cancer (23), head and neck squamous cell carcinoma (24), (gastro)esophageal carcinoma (25,26)) , as well as for any tumor with high tumor mutational burden (TMB-H) (27) or MSI-H/ dMMR (28). It has also been approved for hematologic malignancies, including primary mediastinal large B-cell lymphoma and classical Hodgkin lymphoma (29). The next approval was nivolumab for advanced melanoma (30), followed by the approval for many other tumors (e.g. colorectal cancer (10), esophageal carcinoma (31), pleural mesothelioma (32)), and tumor-agnostic indication with MSI-H/dMMR cancer (33), and Hodgkin lymphoma (29).

Cemiplimab-rwlc, another anti-PD1 mAb, was approved for cutaneous squamous cell carcinoma, basal cell carcinoma, and NSCLC (34,35).

PD-L1 targeting antibodies are being used since 2016, the first approval of atezolizumab. Atezolizumab is approved for many solid tumors (e.g. urothelial carcinoma (36), melanoma, or NSCLC (33)), including a rare pediatric cancer, alveolar soft part sarcoma (37). Avelumab was first approved for a rare skin cancer, Merkel cell carcinoma (38) and later for advanced urothelial and renal cell carcinoma (39). Durvalumab, the third PD-L1 inhibitor, is approved for hepatocellular carcinoma (40), lung cancer (41), biliary tract cancer (42), and endometrial cancer (43).

In 2022, a new type of ICI has been accepted, an antibody targeting lymphocyte-activation gene 3 (LAG-3 or CD223), which is primarly expressed on the surface of $CD4^+$ and $CD8^+$ T cells (44). Upon binding to major histocompatibility complex class II (MHC II), LAG-3 contributes to T cell exhaustion, and frequent co-expression with PD-1 further the limits of antitumoral responses (44). Thus relatlimab, an anti-LAG-3 antibody, when combined with nivolumab, can be more efficient for the treatment of metastatic melanoma (44).

1.3. Immunologically “hot” and “cold” tumors

The tumor microenvironment plays a crucial role in carcinogenesis, tumor invasion, and therapy responses. This complex environment is composed of immune cells (such as T and B cells, natural killer (NK) cells, macrophages, neutrophils, and dendritic cells), stromal cells (including endothelial cells, cancer-associated fibroblasts, and adipocytes), blood vessels, and extracellular matrix components (45). Based on the status of immune cell infiltration, tumors can be classified as either “hot” or “cold” (45).

"Cold" tumors are typically associated with immune escape mechanisms, such as impaired T cell trafficking and infiltration and deficiencies in antigen presentation by tumor cells or dendritic cells (46). When naïve $CD4^+$ T cells (Th0) fail to activate or differentiate properly, antigen presentation by antigen-presenting cells becomes either absent or defective (46).

"Hot" tumors, on the other hand, are characterized by the presence, persistence (due to the absence of apoptotic signals), and functionality (co-stimulatory signals and diverse T cell subsets) of $CD8^+$ T cells in proximity to tumor cells (46). However, the mere presence of $CD8^+$ T cells is insufficient for tumor elimination. Immune-exhausted

and quiescent T cells often show overexpression of LAG-3, PD-1, TIM-3, and TIGIT (T cell immunoreceptor with immunoglobulin and ITIM domain) leading to tumor progression (46). In such cases, NK cell infiltration and its associated cytotoxicity can overcome immune exhaustion and contribute to favourable immune responses (46).

1.4. Therapeutic resistance to immune checkpoint inhibitors

The response rates of ICIs range between 15-60% in different cancers (47), showing 42-45% ORR (objective response rate) in melanoma. More than half of melanoma patients show innate resistance to anti-PD1 therapy, and 25% of treated patients acquire resistance in two years (48). This shows that more robust biomarkers are needed for more specific patient selection, and when needed, ICIs should be used as a combination therapy. The FDA approved three major strategies as companion diagnostic for immune checkpoint inhibitors. These are tumor mutational burden (TMB), microsatellite instability/ mismatch-repair deficiency, and PD-L1 expression (measured either as an immune cell score (IC), tumor proportion score (TPS) or combined proportion score (CPS)) (16). However, PD-L1 and TMB lack accuracy to predict an individual patient's treatment response (16).

Enhancing ICI-responses are achieved in the clinic by combining them with chemotherapy (pemetrexed-platinum), radiotherapy, targeted therapy (atezolizumab plus vemurafenib/ cobimetinib), anti-angiogenic therapy (atezolizumab plus bevacizumab), or other ICI modalities (anti-PD1 plus anti-CTLA-4, anti-PD1 plus anti-LAG-3) (16). Resistance to ICIs is also a complex issue based on intrinsic and extrinsic factors. Tumor cells can have defects in antigen processing and presenting machinery (e.g. MHC-I downregulation), neoantigen loss by immunoediting, immunosuppressive tumor microenvironment such as increased PD-L1 expression, T cell exclusion, the abundance of myeloid-derived suppressor cells (MDSCs), M2-type tumor-associated macrophages, Tregs, cancer-associated fibroblasts (16,49). Changes in the JAK/STAT pathway (interferon signalling), WNT/ß-catenin pathway, or PI3K/AKT/mTOR pathway (e.g. PTEN loss), as well as mutations in RAS genes and cyclin-dependent kinases, also contribute to ICI resistance (16,49). Similarly to metabolic changes, factors such as gut dysbiosis (microbiome), epigenetic remodelling, and co-inhibitory signals (like LAG-3, TIM-3, VISTA, Siglec-15) also play a role (49).

1.5. Yes-associated protein 1 (YAP1) in cancer development

Physiologically, the Hippo-signalling pathway acts as a mechanosensory regulator, integrating physical signals from the plasma membrane and extracellular matrix to cell proliferation, organogenesis, and tissue homeostasis. Thus, the importance of this pathway in cancer development has been widely confirmed, involving tumor suppressive upstream components such as the core serine/threonine kinases MST1/2 (serine/threonine kinase 4/3, alternatively: *STK3/4*), and their binding partner SAV1, which phosphorylate and activate LATS1/2 (large tumor suppressor kinase 1/2) and its binding partners MOB1A/B (50,51). This activation leads to the phosphorylation and cytoplasmic sequestration of downstream oncogenic effector proteins, YAP1 (yes-associated protein 1, also known as *YAP*), and its paralog TAZ (transcriptional coactivator with PDZ-binding motif, also known as *WWTR1*), by 14-3-3 protein, followed by their subsequent proteasomal degradation (50,51). When YAP/TAZ are dephosphorylated, they translocate to the nucleus and interact with the family of TEA domain transcription factors 1-4 (TEAD1, TEAD2, TEAD3, TEAD4) and drive the expression of tumor-promoting genes (50,51). The YAP-TEAD complex interacts with multiple signalling pathways, including the FGFR,- PI3K,- and MAPK cascades. Notably, RAF-1 and MAP4K, both members of MAPK pathway, can interact with MST2, and LATS1/2, respectively (50,52). YAP1 activation can be caused by several reasons e.g. loss-of-function mutations in NF2, MST1/2, LATS1/2 (however mutations in this pathway are rare), YAP/TAZ fusion protein, or mutations in the genes encoding other regulatory signals (e.g. G-protein coupled receptors; RhoA-mediated F-actin polymerization, RAS GTPases, MAPK pathway), and classical pro-oncogenic properties (Warburg-effect, epithelial-mesenchymal-transition) (50).

There are several inhibitors that target YAP and components of the Hippo-YAP signalling pathway, for example CA3, CPD3.I, Super-TDU, flufenamic acid, statins, sitagliptin, verteporfin, and multitarget inhibitors (50,53,54). Verteporfin (VP), an FDA-approved benzoporphyrin derivative, is being used for the treatment age-related macular degeneration (53,55). VP is used as a photosensitizer as it generates reactive oxygen species that leads to cell damage, apoptosis, and anti-angiogenesis. Thus, its antitumor effects were discussed more than ten years ago in a photoactivated manner (56), resulting in multiple clinical trials nowadays for most solid tumors (e.g. NCT03906643). However,

it has been found that VP exerts the same antitumoral effects without photoactivation because it disrupts the YAP/TEAD complex, preventing YAP1 from facilitating the expression of proliferative and survival genes (57–59). Currently, NCT04590664 clinical trial investigating the non-photoactivated form of VP in glioblastoma. Furthermore, VP can sensitize cancer cells to radiotherapy (60), chemotherapy (61), targeted therapy (59), and even anti-PD1 (62).

1.6. Malignant melanoma

Due to environmental and lifestyle changes, incidence of melanoma has been growing gradually however the mortality rates have been declining (1). Notably, it is still one of the most lethal cancers. Malignant melanoma, which has great metastatic potential, is developed from melanoma *in situ* – from benign nevi, or *de novo* upon stress (e.g. UV radiation). Cumulative sun damage typically contributes to *BRAF*-mutant superficial spreading melanoma, lentigo maligna melanoma and desmoplastic melanoma (63). However, non-UV exposed skin, uvea, and mucosa can also transform to malignant melanoma (63,64). For primary melanoma (stage I-II), factors such as lymphovascular invasion, ulcerative tumor, higher Breslow thickness (or Clark's level), higher tumor mitotic rate, melanoma subtype, sentinel lymph node positivity are correlated with worse outcomes. For metastatic melanoma (stage III-IV), pathological biomarkers (e.g. microsatellites, lymph nodes), *BRAF/ NRAS/ NF1/ KIT* mutations, HLA-A/ ROS1/ PRKC fusions, and overall TMB can influence prognosis and therapy response (63). For immune checkpoint inhibitors, evaluating PD-1, PD-L1, CTLA-4, or MHC-I/II levels; tumor-infiltrating lymphocytes (TILs); IFN-γ-associated genes (*IDO1*); and newer biomarkers such as LAG-3, TIM-3, TIGIT, and ICOS is also being explored, with mixed results (63). It is important to note that factors such as age, diet, sex, treatment toxicity, site of tumor and metastases are also clinically useful – but too general – biomarkers (63). Higher YAP/TAZ expression is also associated with advanced TNM stage, increased tumor thickness, deeper invasion, lymph node involvement, (65) and BRAFi-resistance (66).

1.7. High-throughput gene expression techniques – transcriptomics

Global gene expression profiling provides massive, parallel, and quantitative information about the amount and types of RNA in cells and tissues (67).

Microarray technology (also known as a “gene chip” or “DNA chip”) marked the first milestone in the “omics” era, enabling the investigation of mutations, chromosomal alterations, or gene expression. These biological chips contain oligonucleotides fixed to a solid surface, which can be made from glass wafers (microscope slides), silicon wafers, or polymers. The oligonucleotides are either *in situ* synthesised or delivered onto the solid phase (68). Synthesis can be achieved by photolithography (69) (Affymetrix), while delivery can be done via mechanical microspotting (70) (Synteni) or inkjet printing (Incyte Pharmaceuticals, Protogene). The DNA (or cDNA) probes can be immobilized 1 – 500 microns apart, ranging from ~10^5 – 10^7 amplicons/ chip. These fragments hybridize with the corresponding fluorescently labelled “reporter probes” and are scanned by a microscope (71).

RNA sequencing (RNA-Seq) revolutionized transcriptomics by offering unprecedented depth and accuracy through next-generation sequencing. Total RNA or selected species (e.g. polyA-tailed mRNA) are fragmented and converted to cDNA. Adapters are added to the 3’ and/ or 5’ ends, followed by polymerase chain reaction (PCR) for library construction. After clustering, 30–400 bp reads are sequenced from one end (single-end) or both (paired-end) (72). Sequencing can be performed using various methods, including sequencing-by-synthesis (SBS) (e.g. Roche 454, Illumina), sequencing-by-ligation (SBL) (e.g. SOLiD) (73), single-molecule real-time sequencing (SMRT) (e.g. PacBio) (74), nanopore sequencing (e.g. Oxford Nanopore) (75), pyrosequencing (older Roche 454 platforms) (76), and ion semiconductor sequencing (e.g. Ion Torrent) (77).

The NanoString nCounter gene expression system directly measures individual mRNA transcripts without technical bias, ensuring high reproducibility. The process requires two probes: a capture probe with an affinity tag (e.g. biotin), and a reporter probe with a color-coded detection signal. The detection signal consists of uniquely coded, RNA segments with fluorophores. After both probes hybridize with the target mRNA, the tripartite complex undergoes affinity purification, washing, and electrophoresis. The structure is then immobilized in an elongated phase, imaged, and counted for each gene across all field-of-view (78).

2. OBJECTIVES

1. **Establishing a pan-cancer database for immune checkpoint inhibitors.**

My first objective was to identify publicly available gene expression datasets of cancer patients treated with anti-PD1, anti-PD-L1, or anti-CTLA-4 immune checkpoint inhibitors. Eligible datasets with corresponding clinical and survival data (response/ survival outcomes) were collected.

2. **Identifying predictive and pharmacologically targetable biomarkers of immune checkpoint inhibitors.**

By using the established database, the second objective was to find biomarkers of resistance to anti-PD1, anti-PD-L1, and anti-CTLA4 therapies, focusing on those with pharmacological applicability – biomarkers with either *in silico* predicted, *in vitro* or *in vivo* validated inhibitors, or inhibitors approved by health authorities.

3. **Characterization of a clinically relevant, targetable biomarker in a selected tumor.**

My third objective was to narrow down the identified biomarkers to a hit where FDA-approved inhibitor is available – facilitating the rapid clinical translation of results. Followed by the characterization of a selected biomarker in a specified tumor type, where the target is the most robust and the well-supported by the literature.

4. ***In vivo* validation of the identified biomarker to potentiate immune checkpoint inhibitor responses.**

The next aim was to validate the database by testing the previously identified target – demonstrating the benefits of the selected combination therapy in mouse models.

5. **Molecular characterization of tumors following immune checkpoint inhibitor potentiation.**

Lastly, to investigate the molecular mechanisms observed in mice following treatment with an immune checkpoint inhibitor and inhibition of the selected target.

3. METHODS

3.1. Database setup

We searched for datasets using the National Center for Biotechnology Information Gene Expression Omnibus (NCBI GEO) repository (6,79) with the keywords “human [organism] AND (anti-PD1 OR anti-PD-1 OR anti-PD-L1 OR anti-CTLA-4 OR anti-CTLA4)”, and “human [organism] AND (pembrolizumab OR nivolumab OR atezolizumab OR durvalumab OR avelumab OR cemiplimab OR ipilimumab OR camrelizumab OR cintilimab OR tislelizumab OR toripalimab)”. We also used data from the Cancer Research Institute (CRI) iAtlas (80), and conducted a literature search to find eligible studies. Our investigation only included datasets with simultaneously available clinical and bulk-tissue gene expression data (6).

We excluded datasets if either was not available, or when not bulk mRNA expression profiling was performed (e.g. single-cell RNA sequencing, T or B cell receptor sequencing, whole-exome sequencing, non-coding RNA profiling, methylation profiling, protein array) (6,15). Studies using mice, cell lines, immune cells/ blood cells/ normal were also omitted, likewise GEO SuperSeries files. The collected clinical data were a) survival or response data (progression-free survival or interval (PFS/PFI), relapse-free survival (RFS), overall survival (OS), recurrence, and response determined by the Response Evaluation Criteria in Solid Tumors (RECIST)), b) treatment type c) treatment time d) sample characteristics (primary/ recurrence/ metastatic site), e) gender f) metastatic disease g) additional therapies (e.g. targeted or chemotherapy), h) tumor type and site (6,15). By using the published survival/ response time, we categorized patients as responders if they experienced PFS longer than 12 months or had a partial response (PR) or complete response (CR). Those who experienced less than 12 months of PFS or had progressive disease (PD) or stable disease (SD) were categorized as non-responders. Survival time was not used if the patient had no event, and the follow-up time was censored before 12 months (6,15). Tumor samples taken before start of the treatments were termed as “pre-treatment” samples, while tumors collected during or after the therapy were named as “on-treatment” samples (6).

3.2. Web platform integration and statistical analysis

Gene expression data from eligible datasets were combined into a single table, quantile normalized and scaled to 1000 (6,15). To discover differentially expressed genes due to ICI administration, Mann-Whitney-test, ROC curve,- and survival analysis were used. To lower the risk of false discovery by multiple testing, Bonferroni-adjustment ($p = 0.05$) was used due to its stringency and strong control over false positive detection (6).

The ROC plotter platform, running on Ubuntu 20.04.4 LTS server (Apache 2.4.41), was extended to enable the investigation and validation of new biomarkers (6,15). The computations and statistical analyses were performed in R (https://www.r-project.org/) with Bioconductor packages (https://www.bioconductor.org). The analysis platform can be reached at https://rocplot.com/immune.

To associate survival benefits with gene expression patterns, we also integrated our immunotherapy database into the Kaplan-Meier Plotter web service https://kmplot.com/analysis/index.php?p=service&cancer=immunotherapy (6).

3.3. Selection of druggable resistance biomarkers

To discover the strongest candidate that might be eligible for further investigations, three separate analyses were performed using pre-treatment samples of anti-PD1, or anti-PD-L1, or anti-CTLA-4 therapies (6). After applying the Bonferroni correction, we screened the significant, protein-coding genes with a fold change over 1.5 in the non-responder group for druggability. We used PubMed literature search, SelleckChem, GeneCards, and ClinicalTrials to assess druggability and looked for 1) *in silico* predicted drugs, 2) *in vitro* and *in vivo* tested drugs, 3) phase I-II clinical trials, and 4) pharmaceuticals approved by the U.S. Food and Drug Administration (81).

3.4. Cell culture and viability assay

To prove the feasibility of the chosen drug candidate, we used CellTiter-Glo Luminescent Cell Viability assay (Promega, Madison, WI, USA, G7570) on B16-F10 (CRL-6475, manufactured by ATCC (Manassas, VA, USA)), and YUMM1.7 melanoma cell lines (SCC191, Sigma-Aldrich (Burlington, MA, USA)) (81). The cell lines were cultured in DMEM (30-2002, ATCC) supplemented with 10% heat inactivated FBS (30-2020, ATCC), 1% antibiotics/antimycotics (15240062, Thermo Fisher Scientific (Waltham, MA, USA, 10010023)) for B16-F10, and in DMEM/F12 (DF-042-B, Merck

KGaA (Darmstadt, Germany)) with 10% FBS and 1% antibiotics/antimycotics supplemented with 1× non-essential amino acids (TMS-001-C, Merck KGaA) for YUMM1.7 and kept in an incubator at 37°C with 5% CO_2 at 1 atm (81). We plated triplicates of 4000 cells/ well into 96-well plates for overnight adhering. Verteporfin (A12658, Adooq Bioscience (129497-78-5, Irvine, CA, USA)), was added to cell culture medium in light-limited conditions for 24- and 48 hours in 0.1 μM, 0.5 μM, 1 μM, 5 μM, and 10 μM concentrations (81). We used 0.1% DMSO (67-68-5, D2650, Merck KGaA) as a vehicle control, and 10 μM staurosporine (S6942, Merck KGaA) as a positive control. For luminescence measurement, Varioskan LUX plate reader equipped with SkanIt Software 6.0.1 for Microplate Readers RE 6.0.1.6 was used (81). The average relative luminescence units (RLUs) from triplicate measurements of untreated cells were determined, and the RLUs of treated samples were then compared to this baseline to calculate the percentage of viability as the following (81):

$$Cell\ viability\ (\%) = \frac{average\ RLUs\ of\ treated\ cells}{average\ RLUs\ of\ untreated\ cells} \times 100$$

To minimize interference from serum components, triplicates of medium controls were included for background subtraction in all calculations. Outlier analysis was conducted using the ROUT method (Q=1%), followed by a normality test to assess data distribution. Non-parametric Friedman test was performed with post hoc Dunn's test on raw RLU values. All statistical computations were performed in GraphPad Prism (version 8.0.1, GraphPad Software, San Diego, California USA, www.graphpad.com). Independent experiments were conducted for the final evaluation: YUMM1.7 24 h (n = 6), YUMM1.7 48 h (n = 5*),* B16-F10 24 h (n = 5), and B16-F10 48 h (n = 7) (81).

3.5. Mice

The *in vivo* studies were conducted under the 3R-principles (replacement, reduction, refinement) Directive 2010/63/EU of the European Parliament, with a great emphasis placed on animal welfare and environmental enrichment (81). The mice were monitored daily, and their condition was recorded in a log, including the state of their fur, tail, back, and any wounds. If aggression was observed between the animals, they were separated into different cages to prevent further harm. Environmental enrichment (nesting

material, shelter, toys) was provided to promote their quality of life. Food and bedding (SAFE 132) was supplied by SAFE (Société d'Application et de Fabrication d'Ecosystèmes, SAFE Laboratory, France). The mice were moved to a new cage with clean bedding material every 2 to 3 days, maintaining a hygienic environment and reducing the risk of disease.

C57BL/6JRj inbred male mice were obtained from Janvier Labs (France), acclimatized for seven days, and housed in 39.6 cm (l) × 21.5 cm (w) × 17.2 cm (h) cages with individual ventilation (1285L, Techniplast S.p.A.) (81). A maximum of four mice were housed per cage, and ear clipping was used for animal identification. The animals had free access to food and water, maintained on a 12-hour light/dark cycle at 22°C with 40-60% humidity (81).

The experimental procedures were approved by the National Scientific Ethical Committee on Animal Experimentation in Hungary (license no. PE/EA/01017-6/2022) (81).

3.6. Tumor inoculation and treatments

We chose B16-F10 and YUMM1.7 cell lines because of their immunologically "cold" tumor profiles (82,83) and their extensive characterization in the literature, providing a strong foundation for developing our experimental models and methodologies.

Before tumor inoculation, cells were washed, counted using a hemocytometer and LUNA-FX7 Cell Counter (Logos Biosystems, Anyang-si, South Korea), ensuring 80–90% confluency and >80% viability. 500,000 cells were resuspended in 100 µl sterile phosphate buffered saline (PBS) and kept in a syringe on a heated pad to maintain viability (81). Tumors were subcutaneously injected into the rear flank of 8-week-old mice using a 25Gx5/8" needle. Animals were anaesthetised before inoculation with 2% isoflurane (5% induction) (CP-Pharma Handelsgesellschaft mbH, Burgdorf, Germany) using Fluovac Anesthetizing System (Harvard Apparatus, Holliston, MA, USA) (81). Forty-two animals were inoculated with YUMM1.7 cells, while forty-three were inoculated with B16-F10 cells, and monitored daily.

When tumors reached a mean volume of 300 mm^3 (16^{th} day post-inoculation for YUMM1.7, 11^{th} day for B16-F10), the mice were randomly assigned into four groups using a simple random sampling method to minimize initial weight and tumor volume

differences (81). The treatments started on the subsequent days with the following setup: a) 200 µg (1 mg/ml) of IgG2a isotype control antibody (*n* = 10 for YUMM1.7, *n* = 9 for B16-F10) (2A3, BXC-BP0089, Bio X Cell) in a vehicle control (dH_2O, DMSO, Tween80 (Merck KGaA)), b) 200 µg (1 mg/ml) of anti-PD1 (*n* = 9 animals for YUMM1.7 and B16-F10) (RMP1-14, BXC-BP0146, Bio X Cell, Lebanon, NH, USA), c) 50 mg/kg verteporfin (*n* = 9 for YUMM1.7 and B16-F10), d) a combination of verteporfin and anti-PD1 (*n* = 10 for YUMM1.7, *n* = 8 for B16-F10) (81). Treatments were administered every subsequent day intraperitoneally (i.p.) in 200 µl with an insulin syringe. YUMM1.7 mice received seven doses, while B16-F10 mice received only five doses (emergency euthanization due to rapid tumor growth).

Tumor length, tumor width, and body weight were measured on the following days of treatments. If the tumor exceeded 4000 mm^3, reached more than 10% of body weight, caused painful necrotic lesions, or if animals lost over 20% of their weight, they were euthanized under deep anesthesia (90 mg/kg Pentobarbital) by exsanguination (81).

3.7. Statistical analysis of tumor growth

Tumor growth was monitored by calculating tumor volume using length and width measurements from a digital calliper using the ellipsoid formula (84):

$V = \frac{\pi}{6} \times l \times w \times h$, where h=height estimated from length as $H = \frac{2}{3} \times l$

To estimate tumor weight from tumor volume, we used the following formula (81):

$$V\ [mm^3] = \frac{tumor\ weight\ [g]}{1000\ [\frac{g}{mm^3}]}$$

On the day of termination (22nd day for B16-F10, 30th day for YUMM1.7), after euthanasia and tumor dissection, we measured tumors in three dimensions (length, width, height) along with tumor weights. The volumes calculated from the dissected tumors were normalized to body weights and used for statistical computations (81).

To compare treatment groups, an independent t-test was performed with p-value correction in SPSS (IBM Corp. Released 2023. Version 29.0.2.0 Armonk). We used Benjamini-Hochberg (p = 0.05) due to its balance between discovery power and false

discovery rate control, allowing for the detection of more true positives. The following animal numbers were used for statistical evaluation in YUMM1.7 group; a) isotype control (n = 9) b) anti-PD1 (n = 7), b) verteporfin (n = 8), c) verteporfin plus anti-PD1 (n = 9). Statistical evaluation was not conducted for the B16-F10 group (81).

3.8. Histology and immunohistochemistry

Formalin-fixed paraffin-embedded (FFPE) blocks from mice tumors were dissected with a Leica RM2245 microtome (Leica, Wetzlar, Germany); the 4 µm sections were placed onto Apex slides and heated at 60°C for 10 minutes (81). Slides were deparaffinized with xylol (2×10 minutes) and rehydrated in graded concentrations of alcohol: absolute ethanol (2×5 minutes), 96% ethanol (5 minutes), 80% ethanol (5 minutes), 70% ethanol (5 minutes), distilled water (5 minutes).

For haematoxylin-eosin staining, nuclei were stained with Harris haematoxylin (5 minutes), followed by differentiation in 1% acid alcohol (30 seconds). This was followed by counterstaining with eosin (30 seconds), dehydration in 96% ethanol (2×1 minute) and absolute ethanol (2×1 minute), and clearing in xylol (2×5 minutes) (81).

If immunostaining was performed, rehydration was followed by antigen retrieval in Tris buffer (CD3ε staining), or preheated citrate buffer (PCNA staining) for 30 minutes (81). PCNA (proliferating cell nuclear antigen, 13110, D3H8P) and CD3ε (cluster of differentiation 3ε, 99940, D4V8L) rabbit IgG antibodies, were obtained from Cell Signalling Technology (Leiden, The Netherlands). After washing three times with PBS, 3% H_2O_2 was used for peroxidase inactivation, followed by PBS wash for 3×5 minutes. For serum blocking, a mixture of 2.5% normal goat serum and milk powder in PBS was used for CD3ε antibody (1:600). For PCNA antibody dilution (1:4000), 5% normal goat serum in PBS was used. HRP-conjugated anti-rabbit IgG (8114, Cell Signalling Technology) was used as a secondary antibody. Then, slides were washed in gentle shaking with PBS for 3×10 minutes. DAB was used for chromogenic staining as suggested by the manufacturer (SK-4103, Vector Laboratories, Newark, CA, USA). Slides were dehydrated, cleared, and imaged using a Leica LMD6 microscope with a DFC7000 T camera.

3.9. RNA isolation and RT-qPCR

Total RNA was extracted from ~30 mg mouse tumor samples using Qiazol (Qiagen, Venlo, The Netherlands) with chloroform/isopropanol precipitation, and homogenized via TissueLyser (Qiagen, The Netherlands) (81). After centrifugation (10 min, 12,000×g, 4°C), chloroform was added to the supernatant, followed by another centrifugation to separate RNA from DNA and proteins (81). The aqueous phase was used for RNA precipitation with ≥99% isopropanol after centrifugation (15 min, 12,000×g, 4°C). Pellets were washed four times with 75% ethanol, vacuum-dried using a VACUSAFE/VACUBOY system (INTEGRA Biosciences AG, Switzerland), resuspended in RNase-free water, and RNA concentrations were measured with an Implen NanoPhotometer N60 (München, Germany) (81).

SensiFAST cDNA Synthesis Kit (BIO-65053, Bioline, London, UK) was used for cDNA synthesis from 1 µg total RNA with a protocol recommended by the manufacturer (81). The synthesis was carried out using a C1000 Touch Thermal Cycler (Bio-Rad Laboratories, Hercules, CA, USA) under the following conditions: annealing at 25°C for 10 minutes, reverse transcription at 42°C for 15 minutes, and inactivation at 85°C for 5 minutes. The cDNA samples were then diluted to 20× with RNase-free water. RT-qPCR was performed on a LightCycler 480 II instrument (Roche, Basel, Switzerland) using the SensiFAST SYBR No-ROX Kit (BIO-98005, Bioline, London, UK) (81). Initial activation was performed at 95°C for 2 minutes (ramp rate: 4.4°C/s). The amplification phase consisted of 45 cycles with the following conditions: denaturation at 95°C for 5 seconds (ramp rate: 2.2°C/s), annealing at 57°C for 10 seconds (ramp rate: 1.1°C/s), and extension at 72°C for 20 seconds (ramp rate 1.6°C/s). Melting curve analysis was performed starting at 95°C for 1 minute, followed by cooling to 42°C for 2 minutes (ramp rate: 2°C/s), then increasing to 95°C (ramp rate: 0.11°C/s), and ending with cooling to 37°C for 3 minutes (ramp rate: 2.2°C/s). Peptidylprolyl isomerase A (*PPIA*) and hypoxanthine guanine phosphoribosyl transferase (*HPRT*) served as the reference housekeeping genes (81). Relative gene expression was calculated using the $2^{-\Delta\Delta Cp}$ method, where Cp represents the crossing point and the expression of the gene of interest is compared to PPIA, or HPRT and a calibrator sample (81). Primers were purchased from Integrated DNA Technologies (Coralville, IA, USA) (**Table 1**).

Table 1. List of primers used for mice studies. Source: (81).

Gene	Name	Primer sequence	Product size	Tm (°C)	GC%
LY6G	lymphocyte antigen 6 family member G	TTGACAGCATTACCAGTGATCT	121	57.44	40.91
		GCGTTGCTCTGGAGATAGAAG		58.53	52.38
CD86	CD86 antigen	CAGCACGGACTTGAACAACC	144	59.69	55.00
		CTCCACGGAAACAGCATCTGA		60.34	52.38
CD80	CD80 antigen	TTTAGCATCTGCCGGGTGGA	488	61.56	55.00
		CCCCGGTCTGAAAGGACCAG		62.19	65.00
CD3ε	CD3 antigen, epsilon polypeptide	GCGTCTGGTGCCTTCTTCAG	108	61.29	60.00
		CAGGATGCCCCAGAAAGTGT		59.96	55.00
FOXP3	forkhead box P3	TGGCGAAAGTGGCAGAGAG	242	60.00	57.89
		TTGTCAGAGGCAGGCTGGATA		60.90	52.38
CD68	CD68 antigen	TGCGGCTCCCTGTGTGT	61	61.27	64.71
		TCTTCCTCTGTTCCTTGGGCTAT		60.83	47.83
PCNA	proliferating cell nuclear antigen	AGATGTGCCCCTTGTTGTAGAG	148	60.03	50.00
		TGGCATCTCAGGAGCAATCTT		59.44	47.62
PDCD1 (PD-1)	programmed cell death 1	CAAGGACGACACTCTGAAGGAG	89	60.35	54.55
		TCTTCTCTCGTCCCTGGAAGT		59.92	52.38
CD274 (PD-L1)	CD274 antigen	CAGCAACTTCAGGGGGAGAG	176	60.04	60.00
		TTTTGCGGTATGGGGCATTG		59.47	50.00
CD45 (PTPRC)	protein tyrosine phosphatase receptor type C	CCCAGTGATGAACTGAGCACAA	246	60.81	50.00
		GGGATTGTCAGCTTGGCTGC		61.94	60.00
PPIA	peptidylprolyl isomerase A	TATCTGGACTGCCAAGACTGAGTG	127	61.89	50.00
		CTTCTTGCTGGTCTTGCCATTCC		62.23	52.17
YAP1	yes-associated protein 1	CGGCAGGCAATACGGAATATCAA	70	61.36	47.83
		TGCGCAGAGCTAATTCCTGAC		60.74	52.38
HPRT	hypoxanthine guanine phosphoribosyl transferase	GTCCCAGCGTCGTGATTAGC	170	61.15	60.00
		GTGATGGCCTCCCATCTCCT		61.06	60.00

To quantify relative gene expression levels after RT-qPCR, first an outlier analysis (ROUT Q=1%) was performed that was followed by a lognormality test. Either one-way

ANOVA (post-hoc Tukey's) or the Kruskal-Wallis (post-hoc Dunn's) test was used for statistical comparison (81). Analyses were performed GraphPad Prism version 8.0.1 in isotype control (n = 8-9 animals), anti-PD1 (n = 7 animals), verteporfin (n = 6-8 animals), and verteporfin+anti-PD1 (n = 6-9 animals).

4. RESULTS

4.1. *In silico* discovery

4.1.1. Integrative database of immune-checkpoint inhibitor treated cancer patients

225 series files were identified with the utilization of NCBI GEO and 6 datasets from the CRI iAtlas. Additionally, 5 extra cohorts were found by looking up the referenced literature (85–89), leading to 246 datasets with 3,823 samples to be screened. A detailed description of the complete screening process can be seen in **Figure 1**.

After omitting datasets with unfitting or duplicated data, we manually screened 1,502 samples. Of which, 68 samples were excluded due to (1) duplicated sample of a patient, (2) irrelevant treatment (not ICI), (3) no response or survival data, (4) no expression data, (5) ambiguous treatment time, (6) not available on iAtlas (if the rest of the dataset was used from iAtlas), (7) not primary tumor, (8) low sample size of a given tumor. The final database consists of 1,434 samples from 19 datasets (**Figure 1**).

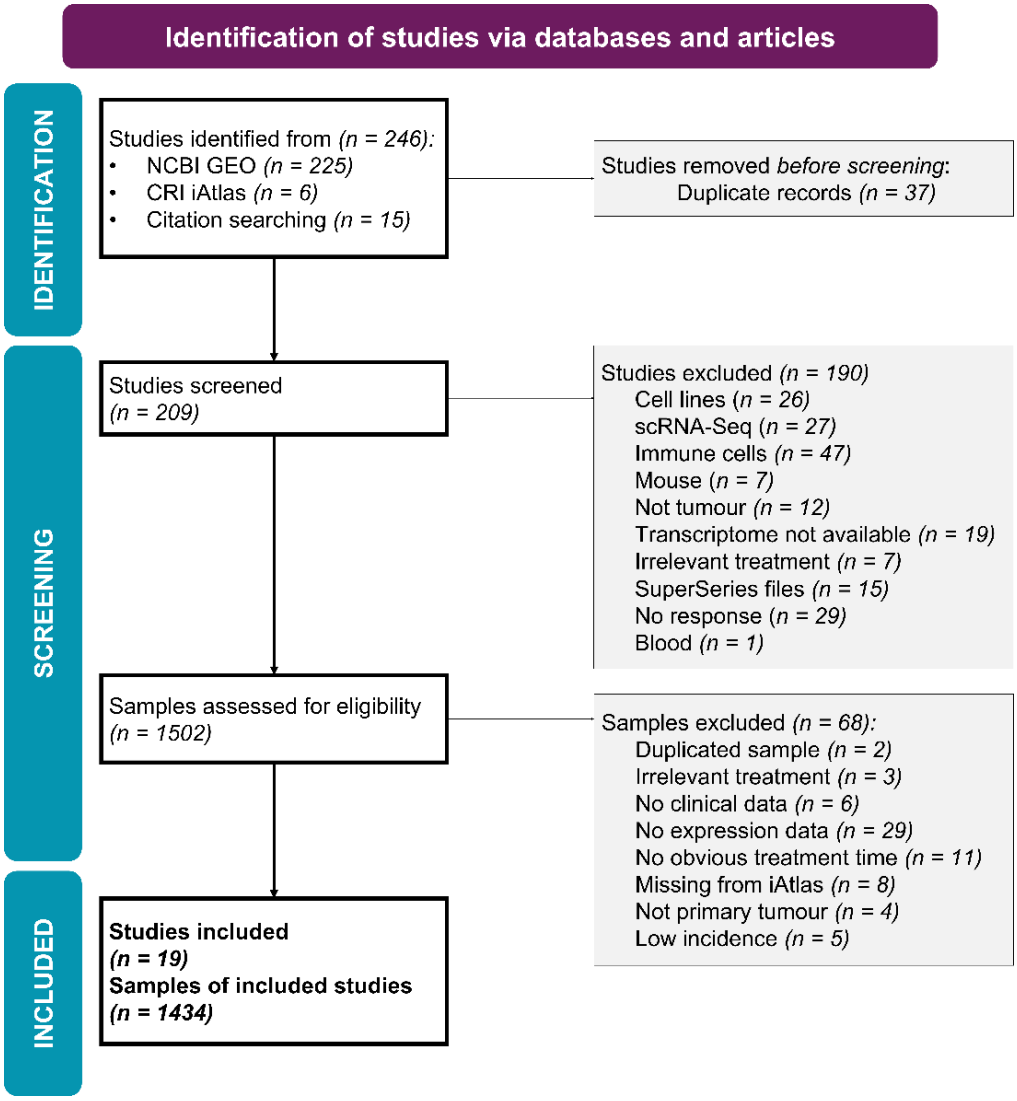

Figure 1. PRISMA flowchart showing the database setup for immune checkpoint inhibitor-treated cancer patients. White boxes indicate included studies or samples, while grey boxes represent excluded ones.

This database was integrated to www.rocplot.com/immune ROC Plotter Immunotherapy analysis platform (**Figure 2**) consisting of melanoma (n = 570), urothelial cancer (bladder/ureter/pelvis cancer) (n = 438), head and neck squamous cell carcinoma (n = 110), esophageal and gastroesophageal junction adenocarcinoma (n = 103), lung cancer (small cell and non-small-cell lung cancer, or squamous and non-squamous non-small cell lung cancer) (n = 60), gastric cancer (n = 45), renal cell carcinoma (n = 44), glioblastoma (n = 28), hepatocellular carcinoma (n = 22), breast cancer (triple-negative (n = 12), and ER+HER2- breast cancer (n = 2)) (**Figure 3**) (6).

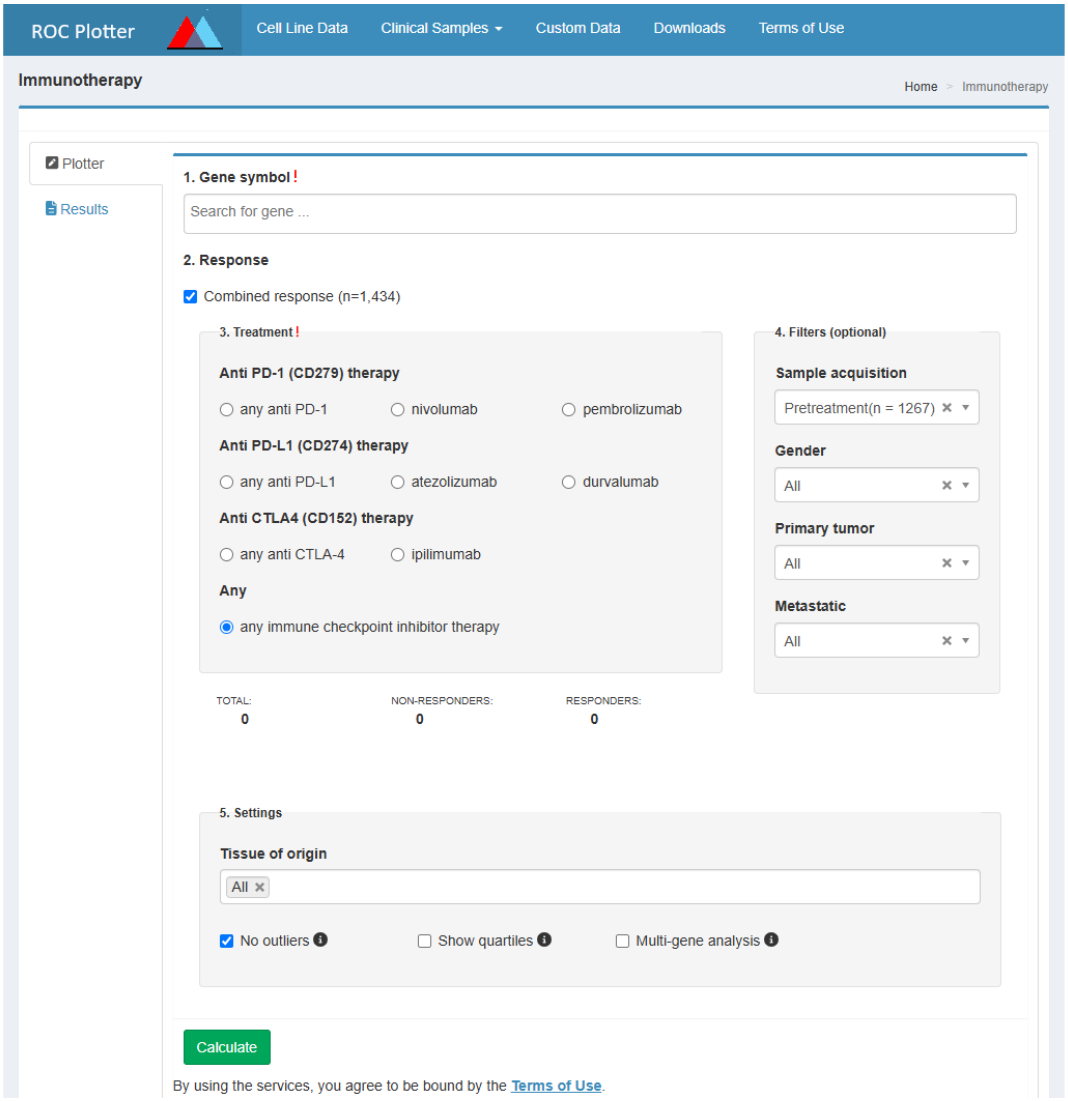

Figure 2. Web platform design of www.rocplot.com/immune. Landing page of the ROC Plotter Immunotherapy platform with options to search for a gene or multiple genes simultaneously, select treatments and tumor types, and apply additional filters (*sample acquisition, gender, primary tumor sample, metastatic disease*).

Patients either received anti-PD1 (nivolumab, or pembrolizumab) (all n = 877; pre-treatment n = 776; on-treatment n = 101), anti-PD-L1 (atezolizumab, or durvalumab) (all n = 488; pre-treatment n = 457; on-treatment n = 31), or anti-CTLA-4 (ipilimumab) (all n = 124; pre-treatment n = 98; on-treatment n = 26) treatments, or n = 55 combination therapy (**Figure 3**) (6). The description of the datasets was thoroughly discussed in our previous review article (15).

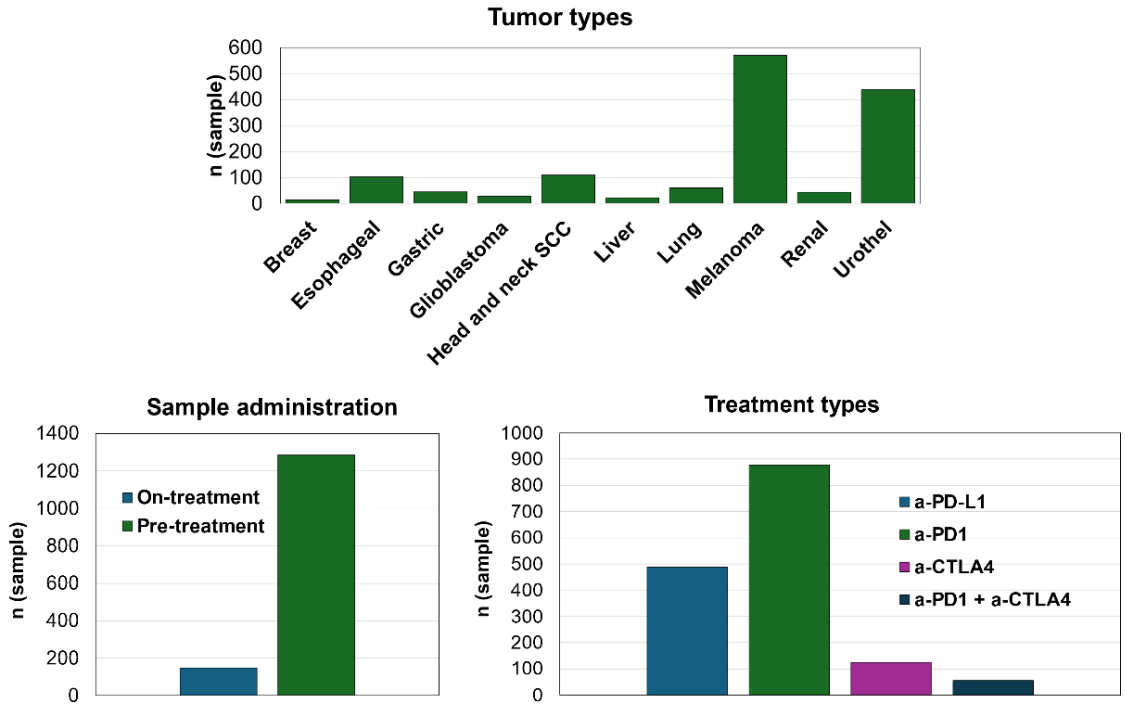

Figure 3. Final database structure and sample distribution (*n* = 1,434). Number of samples for each tumor type (**above**), overall distribution of samples collected before (*pre-treatment*) and after (*on-treatment*) ICI administration (**bottom, left**). Number of samples corresponding to different treatment regimens (*anti-PD1, anti-PD-L1, anti-CTLA-4, or combination of them*) (**bottom, right**).

4.1.2. Pan-cancer biomarkers of anti-PD1, anti-PD-L1, and anti-CTLA-4 baseline resistance with pharmacological interventions

The following nineteen datasets were included for 1) anti-PD1 pre-treatment group: GSE78220, GSE91061, GSE93157, GSE115821, GSE121810, GSE136961, GSE140901, GSE165745, GSE176307, Cristescu2018 (90), Gide2019 (91), Kim2018 (87), Miao2018 (88), Liu2019 (89); 2) anti-PD-L1 pre-treatment group: GSE165252, GSE176307, GSE183924, Mariathasan2018 (92), Miao2018; and 3) anti-CTLA-4 pre-treatment group: GSE115821, GSE140901, GSE165278, Gide2019, Miao2018, VanAllen2015 (93). Different technological approaches were utilized in the involved studies such as RNA-sequencing (Illumina, or Ion Torrent platforms), and NanoString nCounter platforms, and the datasets were involved regardless of tumor type (**Table 2**) (6).

Table 2. Final database of immune checkpoint inhibitor-treated cancer patients with transcriptomic and clinical data. Source: (6).

Dataset ID	Sample	Tumor	Treatment	Acquisition	Outcome	Platform
GSE78220	28	Melanoma	Pembrolizumab	Pre-treatment	OS and response by RECIST	RNA-Seq (Illumina HiSeq 2000)
GSE91061	98	Melanoma	Nivolumab	Pre-treatment or On-treatment	OS and response by RECIST	RNA-Seq (Illumina Genome Analyzer)
GSE93157	5	Head and Neck Squamous Cell Carcinoma	Nivolumab	Pre-treatment	PFS and response by RECIST	NanoString nCounter PanCancer Immune Profiling Panel
	22	Non-Squamous Non-Small Cell Lung Cancer	Nivolumab or Pembrolizumab	Pre-treatment	PFS and response by RECIST	
	25	Skin Cutaneous Melanoma	Nivolumab or Pembrolizumab	Pre-treatment	PFS and response by RECIST	
	13	Squamous Non-Small Cell Lung Cancer	Nivolumab or Pembrolizumab	Pre-treatment	PFS and response by RECIST	
GSE115821	37	Melanoma	Anti-PD1 and/ or Anti-CTLA-4	Pre-treatment or On-treatment	Response	RNA-Seq (Illumina HiSeq 2000 and Illumina NextSeq 500)
GSE121810	28	Glioblastoma	Pembrolizumab	Pre-treatment or On-treatment	PFI, OS, response by RECIST	RNA-Seq (Illumina HiSeq 3000)

GSE136961	21	Non-Small-Cell Lung Cancer	Anti-PD1	Pre-treatment	PFS, OS	RNA-Seq (Ion Torrent S5 XL)
GSE140901	22	Hepatocellular Carcinoma	Nivolumab and/ or Ipilimumab	Pre-treatment	PFS, OS, response by RECIST	NanoString nCounter PanCancer Immune Profiling Panel
GSE165252	66	Esophageal Adenocarcinoma	Atezolizumab	Pre-treatment or On-treatment	PFS, OS, and response	RNA-Seq (Illumina HiSeq 4000)
GSE165278	21	Melanoma	Ipilimumab	Pre-treatment or On-treatment	OS	RNA-Seq (Illumina HiSeq 2500)
GSE165745	24	Melanoma	Pembrolizumab or Nivolumab	Pre-treatment	Response	NanoString nCounter Vantage 3D Human Wnt Pathways Panel
GSE176307	84	Bladder/ Ureter/ Pelvis Cancer	Pembrolizumab/ Nivolumab, or Atezolizumab/ Durvalumab	Pre-treatment	PFS and response by RECIST	RNA-Seq (Ion Torrent S5 XL)
GSE183924	37	Esophageal and Gastroesophageal Junction Adenocarcinoma	Durvalumab	Pre-treatment	RFS	RNA-Seq (Illumina NovaSeq 6000)
Cristescu2018	17	Bladder Cancer	Pembrolizumab	Pre-treatment	Response	NanoString nCounter
	12	Triple Negative Breast Cancer	Pembrolizumab	Pre-treatment	Response	

	2	ER+HER2- Breast Cancer	Pembrolizumab	Pre-treatment	Response	
	105	Head and Neck Squamous Cell Carcinoma	Pembrolizumab	Pre-treatment	Response	
	86	Melanoma	Pembrolizumab	Pre-treatment	Response	
	4	Small Cell Lung Cancer	Pembrolizumab	Pre-treatment	Response	
Gide2019	88	Melanoma	Pembrolizumab and/ or Nivolumab and/ or Ipilimumab	Pre-treatment	PFI, OS, response by RECIST	RNA-Seq (Illumina HiSeq 2500)
Kim2018	45	Gastric Cancer	Pembrolizumab	Pre-treatment	Response by RECIST	RNA-Seq (Illumina NextSeq 550)
Liu2019	121	Melanoma	Nivolumab or Pembrolizumab	Pre-treatment	PFS, OS, response by RECIST	RNA-Seq (Illumina HiSeq 2000 v3, HiSeq 2500)
Mariathasan2018	348	Urothelial Cancer	Atezolizumab	Pre-treatment	OS and response by RECIST	RNA-Seq (Illumina TruSeq RNA Access)
Miao2018	33	Renal Cell Carcinoma	Nivolumab and/ or Ipilimumab, or Atezolizumab	Pre-treatment	PFS, OS, and response by RECIST	RNA-Seq (Illumina HiSeq 2000 v3, HiSeq 2500)
VanAllen2015	42	Melanoma	Ipilimumab	Pre-treatment	PFS, OS, and response by RECIST	RNA-Seq (Illumina HiSeq 2500)

In the anti-PD1 pre-treatment group, ROC AUC and p-values of 29,755 genes were analyzed (6). After applying Bonferroni correction (p < 1.6E-06) to mitigate false discoveries, 912 genes remained significant. We investigated only those genes that showed FC > 1.5 in non-responding patients, including *STK35* (FC = 1.7, AUC = 0.651, p = 1.4E-08), *SPIN1* (FC = 1.6, AUC = 0.682, p = 9.1E-12), *SRC* (FC = 1.6, AUC = 0.667, p = 5.9E-10), *SETD7* (FC = 1.7, AUC = 0.663, p = 1.0E-09), *TEAD3* (FC = 1.7, AUC = 0.649, p = 4.1E-08), *FGFR3* (FC = 2.1, AUC = 0.657, p = 3.7E-09), *YAP1* (FC = 1.6, AUC = 0.655, p = 6.0E-09), and *BCL2* (FC = 2.2, AUC = 0.634, p = 9.7E-08) (6). Interestingly, most of these genes were connected to *YAP1* regulation, particularly *SRC* (94,95), *SETD7* (96), *BCL2* (97), *STK35* (98), *FGFR3*, and *TEAD3*.

In the anti-PD-L1 pre-treatment group, 26,819 genes were analyzed, and 38 hits were significant (p < 1.8E-06). We found no tumor-agnostic, upregulated, druggable genes of resistance (6).

In the anti-CTLA-4 pre-treatment group, 22,561 genes were analyzed, yielding 80 significant genes. Among them, only *BLCAP* (FC = 1.7, AUC = 0.735, p = 2.1E-06) was identified as a druggable gene overexpressed in the pan-cancer cohort of non-responding patients (6).

4.1.3. Predictive biomarkers of anti-PD1 resistance in melanoma

To identify a suitable target for validation, we first examined which tumor type and treatment were the most frequently represented in the database, which was the melanoma anti-PD1 pre-treatment (n = 415) (**Figure 3**). Since immune checkpoint inhibitors are primarily utilized as adjuvant therapies in melanoma, analyzing pre-treatment cohorts provides a more accurate representation of their clinical relevance.

We then re-ran ROC and Mann-Whitney tests and performed a survival analysis using the following datasets: GSE91061, GSE93157, GSE78220, GSE165745, GSE115821, CRISTESCU2018, GIDE2019, LIU2019. After Bonferroni-correction, twenty-one genes showed significant overexpression in the anti-PD1 resistant melanoma group (**Table 3**). Among these, we found available inhibitors for six targets: *YAP1*, spindlin 1 (*SPIN1*), eukaryotic translation initiation factor 4H (*EIF4H*), solute carrier family 25 member 36 (*SLC25A36*), lysophospholipase 1 (*LYPLA1*), and GID complex subunit 4 homolog (*GID4*) (81).

Table 3. Twenty-one genes with overexpression in anti-PD1 non-responding melanoma patients (*FC = fold change, MW=Mann-Whitney*). Source: (81).

gene symbol	FC in non-responders	MW p-value	ROC AUC	ROC AUC p-value	inhibitor
SPIN1	1.57	3.22E-07	0.678	1.30E-08	compound 3 (MS31)
GID4	1.50	4.37E-07	0.676	3.30E-08	Compounds 16, 67, and 88
LYPLA1	1.60	8.99E-07	0.671	5.80E-08	ML211 and acyl piperidine 21
EIF4H	1.54	1.17E-06	0.669	1.10E-07	pateamine
SLC25A36	1.64	1.73E-08	0.696	2.50E-10	tannic acid and 4,7-diphenyl-1,10-phenanthroline
YAP1	1.85	1.07E-08	0.699	7.50E-11	verteporfin, CA3, statins, or A35
EPN2	2.52	2.28E-07	0.680	1.00E-08	N/A
LEPROT	1.87	1.38E-07	0.683	4.30E-09	N/A
PRRG1	1.86	5.54E-08	0.689	1.20E-09	N/A
TMEM263	1.85	2.42E-07	0.68	8.40E-09	N/A
C5orf24	1.85	2.43E-09	0.707	8.10E-12	N/A
HACD3	1.73	1.50E-07	0.693	2.80E-09	N/A
KCTD15	1.73	4.45E-07	0.676	2.80E-08	N/A
MPZL1	1.70	8.72E-07	0.671	5.10E-08	N/A
PCMTD2	1.68	1.89E-07	0.681	7.00E-09	N/A
VMA21	1.67	7.49E-07	0.672	5.30E-08	N/A
CLDN12	1.62	5.38E-07	0.674	5.10E-08	N/A
PLS3	1.58	2.90E-07	0.678	1.90E-08	N/A
MTURN	1.55	2.08E-07	0.681	9.90E-09	N/A
GZF1	1.53	7.40E-07	0.672	5.20E-08	N/A
TIGD7	1.52	3.53E-07	0.677	2.60E-08	N/A

4.1.4. Yes-associated protein 1 (YAP1) as a druggable, predictive, and prognostic biomarker of anti-PD1 resistance in melanoma

In the anti-PD1 pre-treated melanoma cohort, *YAP1* emerged as the most promising target (FC = 1.85, Mann-Whitney p-value = 1.07E-08, AUC = 0.699, ROC AUC p-value = 7.50E-11) (**Table 3, Figure 4C, 4D**) as other potential druggable candidates were either less studied in malignant tumors, faced concerns about off-target effects, or were still in early drug development (81). In contrast, *YAP1* is a well-established oncogene, particularly in skin cutaneous melanoma, and has a clinically approved inhibitor, verteporfin (81). The advantage of using drugs already utilized in clinical practice is that there is no need to navigate the long and quite unsuccessful path of drug development. In oncology, the probability of a drug progressing from Phase 1 to approval is only 3.4% (99). Additionally, *YAP1* inhibitors are currently being evaluated for antitumor effects in several clinical trials.

We validated *YAP1* in this cohort as a prognostic biomarker using KM-plotter service. Survival analysis showed that higher *YAP1* expression correlates with poorer progression-free survival (HR = 2.51, p = 1.2E-06), and overall survival (HR = 2.15, p = 1.2E-05) (**Figure 4A, 4B**) (81). Based on the robust predictive and prognostic capabilities of *YAP1*, we chose this target for *in vitro* and *in vivo* validation using verteporfin inhibitor (81).

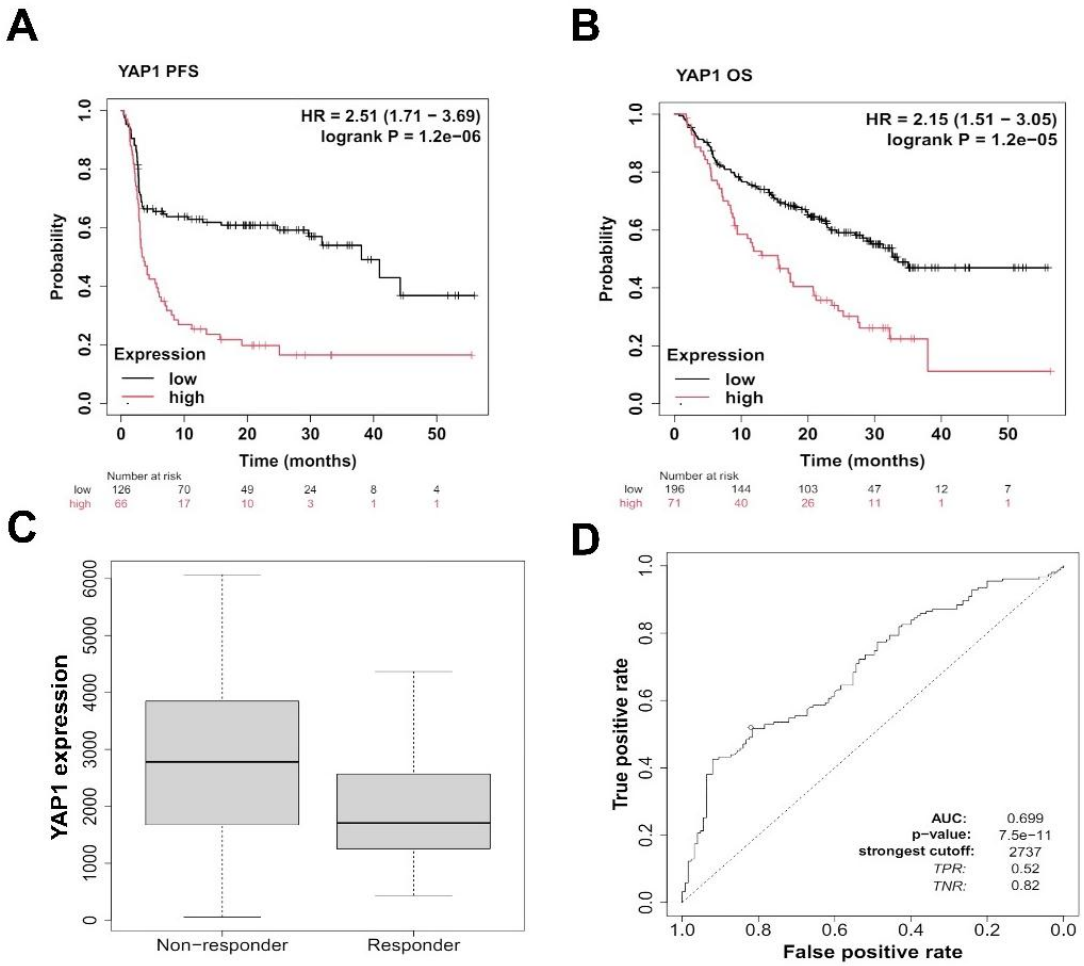

Figure 4. Evaluation of *YAP1* as a predictive and prognostic biomarker in the anti-PD1 pre-treatment melanoma cohort. YAP1 overexpression correlation with worse progression free survival (**A**), and overall survival (**B**), and therapy resistance (**C**) with corresponding ROC curve (**D**). Source: (81).

4.2. *In vitro* and *in vivo* validation

4.2.1. Yes-associated protein 1 (YAP1) inhibition with verteporfin in melanoma cells

We assessed the effects of verteporfin (VP) on YUMM1.7 and B16-F10 melanoma cell viability using a luminescent assay. Only the highest VP concentration (10 μM) showed a significant reduction in viability after 24 hours, compared to both untreated cells ($p = 0.0378$) and the vehicle control ($p = 0.0019$) in B16-F10 (**Figure 5A, 5B, 5D, 5E**) (81). Conversely, in YUMM1.7 cells, 5 μM VP was also effective, significantly decreasing viability compared to untreated ($p = 0.0305$) and vehicle control cells ($p =$

0.0001) (**Figure 5A, 5C, 5F, 5G)**. Extending the incubation period to 48 hours enhanced the treatment in both cell lines. Notably, 1 µM VP significantly reduced cell viability in B16-F10 (p = 0.0210) and YUMM1.7 (p = 0.0030) cells (81). These findings indicate that verteporfin treatment effectively decreases cell viability in our tumor models and YUMM1.7 showing greater susceptibility to VP.

A

24 h	1	2	3	4	5	6	7	8	9	10	11	12
A												
B		B16-F10 *Untreated*	B16-F10 *0.1 µM VP*	B16-F10 *1 µM VP*	B16-F10 *10 µM VP*	*Medium*	YUMM1.7 *Untreated*	YUMM1.7 *0.1 µM VP*	YUMM1.7 *1 µM VP*	YUMM1.7 *10 µM VP*	*Medium*	
C		B16-F10 *Untreated*	B16-F10 *0.1 µM VP*	B16-F10 *1 µM VP*	B16-F10 *10 µM VP*	*Medium*	YUMM1.7 *Untreated*	YUMM1.7 *0.1 µM VP*	YUMM1.7 *1 µM VP*	YUMM1.7 *10 µM VP*	*Medium*	
D		B16-F10 *Untreated*	B16-F10 *0.1 µM VP*	B16-F10 *1 µM VP*	B16-F10 *10 µM VP*	*Medium*	YUMM1.7 *Untreated*	YUMM1.7 *0.1 µM VP*	YUMM1.7 *1 µM VP*	YUMM1.7 *10 µM VP*	*Medium*	
E		B16-F10 *Vehicle*	B16-F10 *0.5 µM VP*	B16-F10 *5 µM VP*	B16-F10 *Positive*		YUMM1.7 *Vehicle*	YUMM1.7 *0.5 µM VP*	YUMM1.7 *5 µM VP*	YUMM1.7 *Positive*		
F		B16-F10 *Vehicle*	B16-F10 *0.5 µM VP*	B16-F10 *5 µM VP*	B16-F10 *Positive*		YUMM1.7 *Vehicle*	YUMM1.7 *0.5 µM VP*	YUMM1.7 *5 µM VP*	YUMM1.7 *Positive*		
G		B16-F10 *Vehicle*	B16-F10 *0.5 µM VP*	B16-F10 *5 µM VP*	B16-F10 *Positive*		YUMM1.7 *Vehicle*	YUMM1.7 *0.5 µM VP*	YUMM1.7 *5 µM VP*	YUMM1.7 *Positive*		
H												

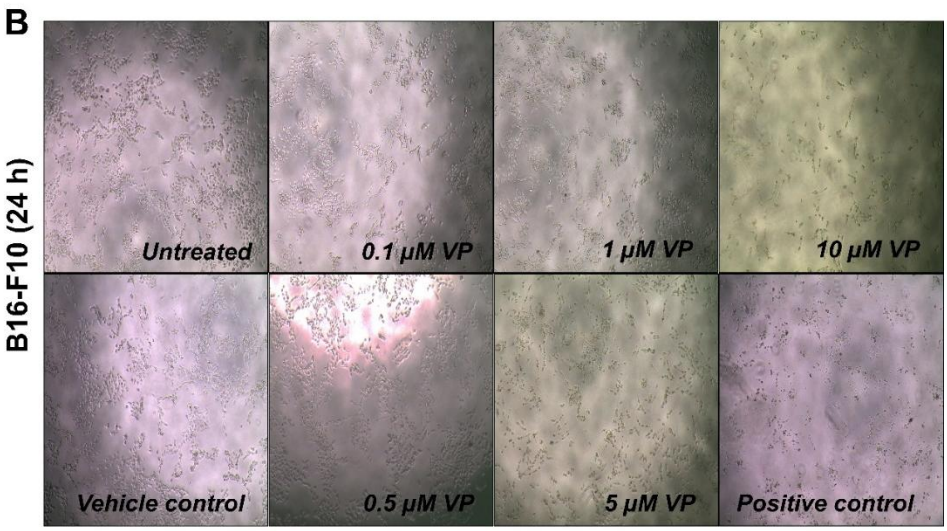

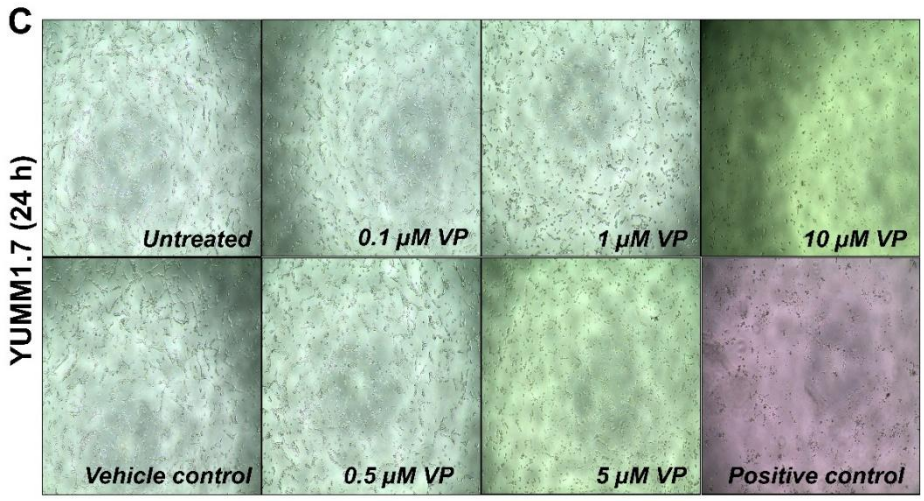

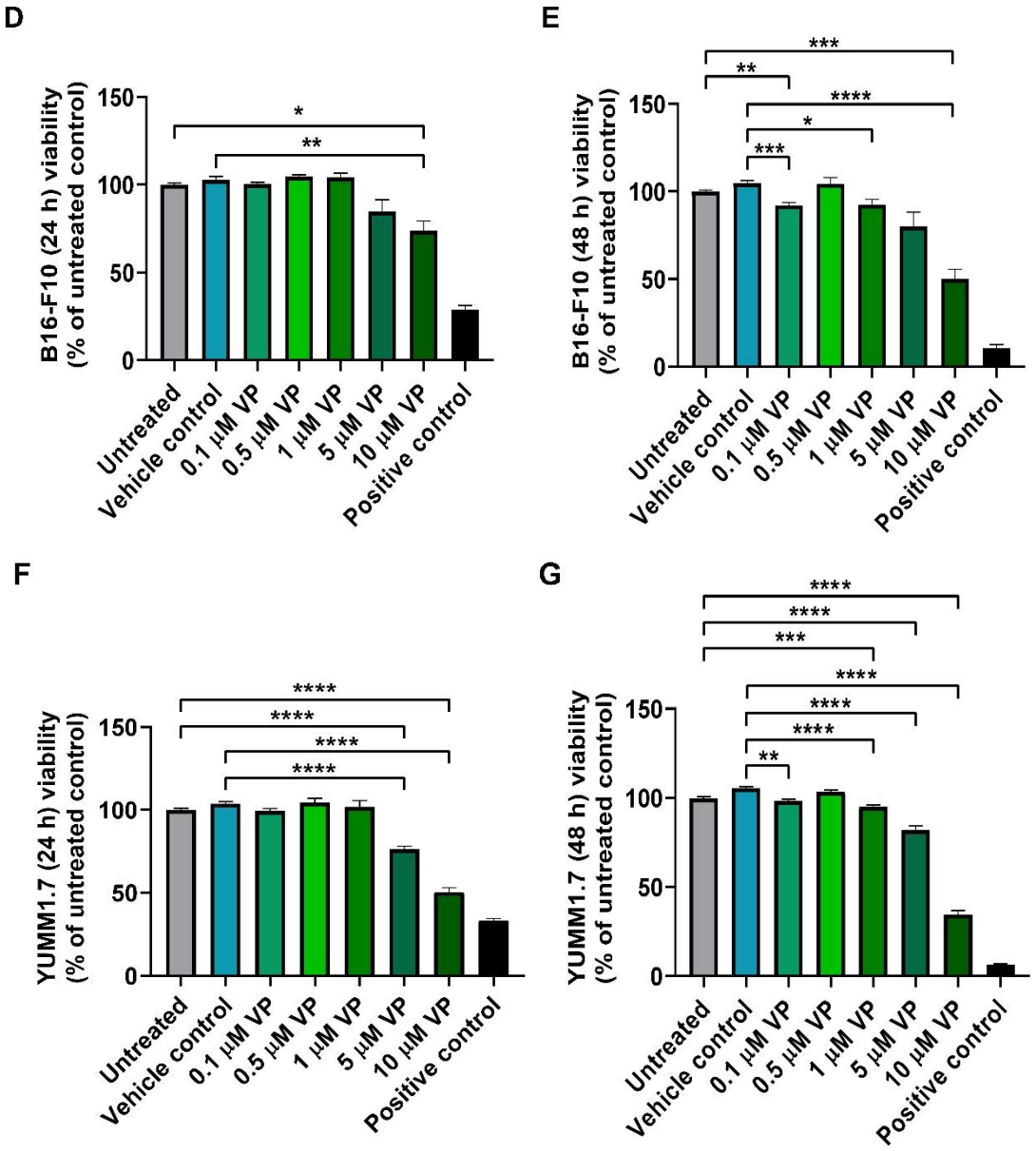

Figure 5. Plate layout of viability assay (**A**) and representative microscopic photos taken after 24 hours of treatment in a selected well of B16-F10 cells (**B**) or YUMM1.7 cells (**C**). Effects of verteporfin on B16-F10 cells after 24 h (**D**) or 48 h (**E**), and on YUMM1.7 cells after 24 h (**F**) or 48 h (**G**) incubation. Independent experiments used for Friedman test: B16-F10 24 hours (n = 5), B16-F10 48 hours (n = 7), YUMM1.7 24 hours (n = 6), YUMM1.7 48 hours (n = 5). *$P \leq 0.05$, **$P \leq 0.01$, ***$P \leq 0.001$, ****$P \leq 0.0001$. Source: (81).

4.2.2. Verteporfin potentiates anti-PD1 therapy in mice bearing *BRAF*^{V600E} mutations in melanoma

To investigate whether YAP1 inhibition could enhance the efficacy of anti-PD1 therapy in melanoma, we treated C57BL/6J mice bearing YUMM1.7, and B16-F10 tumors with the following regimens: 200 µg isotype control, 200 µg anti-PD1, 50 mg/kg verteporfin, and a combination of verteporfin+anti-PD1 (81). Tumor volumes in the YUMM1.7-inoculated verteporfin+anti-PD1 group were significantly smaller compared to the isotype control ($p = 0.021$, adjusted $p = 0.063$) and the anti-PD1 monotherapy group ($p = 0.008$, adjusted $p = 0.048$) (**Figure 6A**) (81). However, neither verteporfin alone ($p = 0.425$) nor anti-PD1 alone ($p = 0.971$) showed a significant advantage over the control group (81). While verteporfin monotherapy appeared more effective than anti-PD1, the difference was not statistically significant ($p = 0.363$ vs. anti-PD1; $p = 0.083$ vs. combination therapy) (**Figure 6A**) (81). The combination therapy led to the most substantial decrease in tumor weight (mean ± SD: 1.738 g ± 0.73) compared to anti-PD1 (2.609 g ± 0.78) ($p = 0.038$) (81). We did not find significant differences between verteporfin (2.238 g ± 0.95), or the isotype control groups (2.630 g ± 1.36) in YUMM1.7 tumor mass (**Figure 6A**) (81).

Mice inoculated with B16-F10 melanoma tumors exhibited rapid tumor progression, rendering them unresponsive to all treatments thus early euthanasia was required, leading to small sample size at the end of the study ($n = 3$ isotype control, $n = 3$ anti-PD1, $n = 1$ verteporfin, $n = 2$ verteporfin+anti-PD1) (**Figure 6B**). Thus, data was not evaluated in the B16-F10 group.

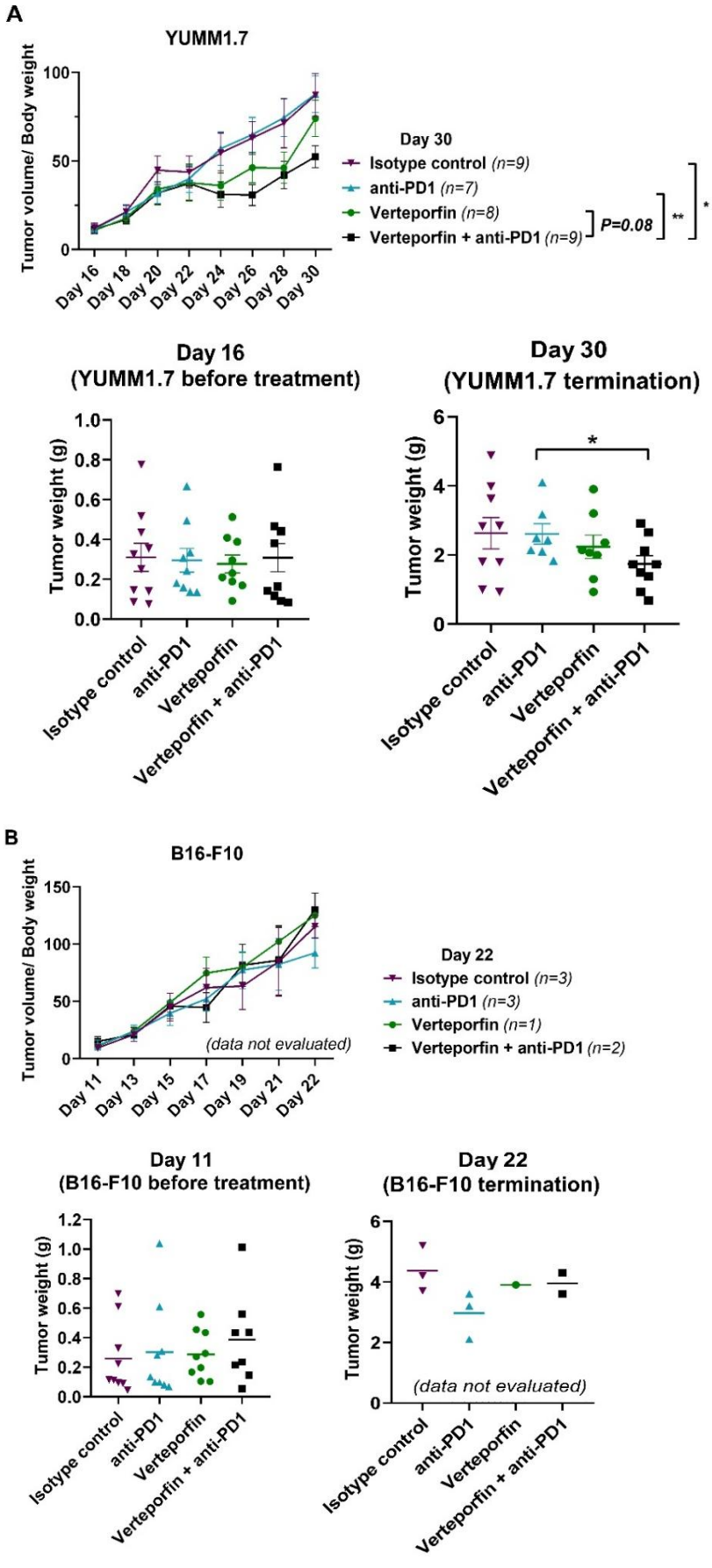
A
YUMM1.7
Tumor volume/ Body weight
100
50
0
Day 16
Day 18
Day 20
Day 22
Day 24
Day 26
Day 28
Day 30
Day 30
Isotype control (n=9)
anti-PD1 (n=7)
Verteporfin (n=8)
Verteporfin + anti-PD1 (n=9)
P=0.08
**
*
Day 16
(YUMM1.7 before treatment)
Tumor weight (g)
1.0
0.8
0.6
0.4
0.2
0.0
Isotype control
anti-PD1
Verteporfin
Verteporfin + anti-PD1
Day 30
(YUMM1.7 termination)
Tumor weight (g)
6
4
2
0
*
Isotype control
anti-PD1
Verteporfin
Verteporfin + anti-PD1
B
B16-F10
Tumor volume/ Body weight
150
100
50
0
(data not evaluated)
Day 11
Day 13
Day 15
Day 17
Day 19
Day 21
Day 22
Day 22
Isotype control (n=3)
anti-PD1 (n=3)
Verteporfin (n=1)
Verteporfin + anti-PD1 (n=2)
Day 11
(B16-F10 before treatment)
Tumor weight (g)
1.2
1.0
0.8
0.6
0.4
0.2
0.0
Isotype control
anti-PD1
Verteporfin
Verteporfin + anti-PD1
Day 22
(B16-F10 termination)
Tumor weight (g)
6
4
2
0
(data not evaluated)
Isotype control
anti-PD1
Verteporfin
Verteporfin + anti-PD1

Figure 6. Tumor growth in YUMM1.7 **(A)**, and B16-F10 **(B)**. Upper plots show body weight-normalized tumor volume growth. Individual dots show the mean values of treatment groups with ±SEM. Tumor weights before treatments were predicted from tumor volumes as: V[mm^3]=weight[g]/1000[g/mm^3]. Each dot represents an individual animal with mean values as lines (bottom plots). *$P \leq 0.05$, **$P \leq 0.01$, ***$P \leq 0.001$, ****$P \leq 0.0001$. Source: (81).

Given the strong contrast in treatment responses between the YUMM1.7 and B16-F10 models, we examined *YAP1* expression in these tumors. YUMM1.7 tumors exhibited significantly higher *YAP1* expression compared to B16-F10 tumors, with significant differences observed in both the isotype control groups (p = 0.003) and the anti-PD1-treated groups (p = 0.001) (**Figure 7**) (81). However, anti-PD1 monotherapy did not directly affect *YAP1* expression in either tumor model.

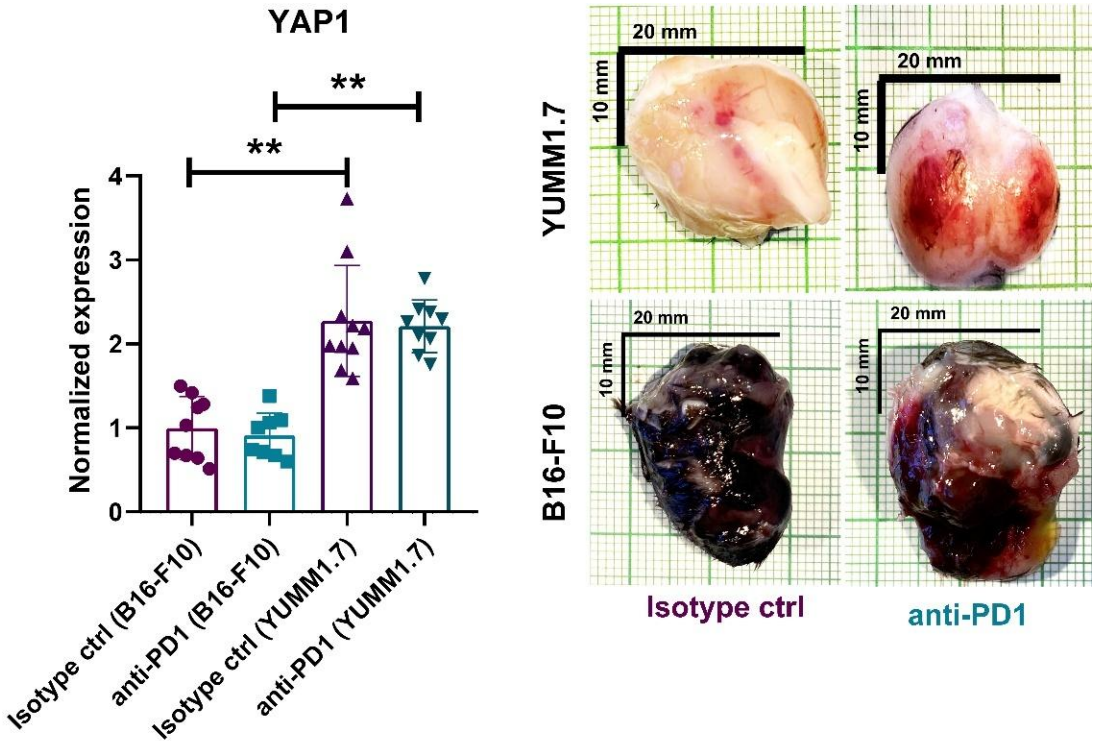

Figure 7. YAP1 expression after anti-PD1 treatment (*left*) in YUMM1.7 and B16-F10 mice with corresponding, representative pictures of dissected tumors (*right*). RT-qPCR data are visualized as normalized $2^{-\Delta\Delta Cp}$ values, and Kruskal-Wallis (post hoc Dunn's) was used for the calculation. *$P \leq 0.05$, **$P \leq 0.01$. Source: (81).

These results suggest that the presence of *BRAF* mutations in YUMM1.7 tumors contribute to higher *YAP1* expression, enhancing their response to verteporfin while simultaneously driving resistance to anti-PD1 therapy. In contrast, B16-F10 tumors, which are wild-type for *BRAF*, remain unresponsive to the mentioned treatments.

4.2.3. Verteporfin plus anti-PD1 combination therapy shifts immunologically "cold" tumors to "hot"

Next, we analyzed dissected tumor samples from YUMM1.7-inoculated mice to evaluate proliferative and immune infiltrative characteristics. Hematoxylin & eosin staining, along with the proliferation marker PCNA, confirmed a high density of tumor cells across all treatment groups, with no discernible effect on proliferation (**Figure 8A**). Representative images of CD3ε immunostaining (**Figure 8B**) and RT-qPCR (**Figure 9**), which showed significantly increased *CD3ε* expression in the verteporfin+anti-PD1 group compared to the isotype control ($p = 0.047$), suggest that the combination therapy promotes an immunologically active tumor microenvironment (81).

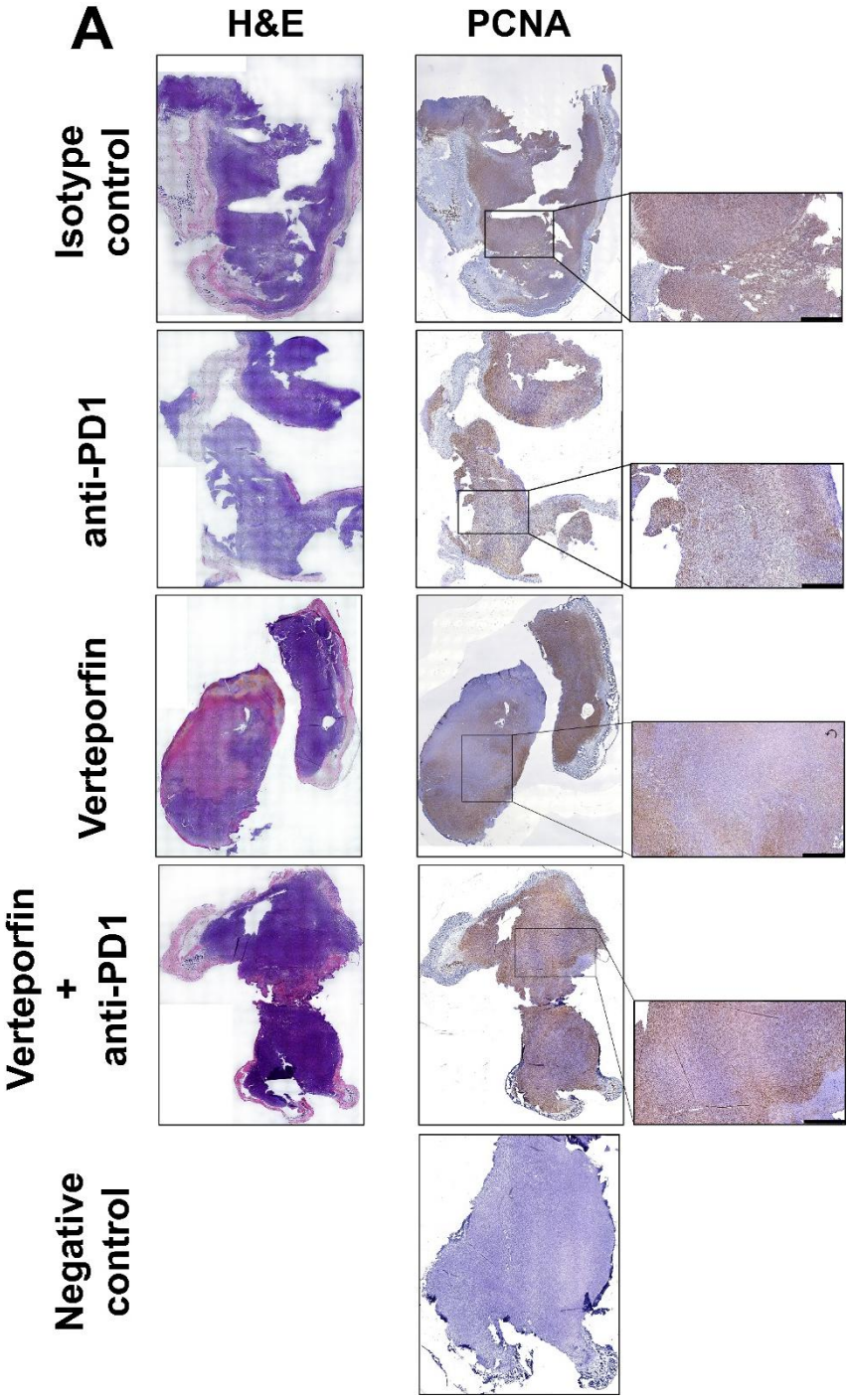
A
H&E
PCNA
Isotype control
anti-PD1
Verteporfin
Verteporfin + anti-PD1
Negative control

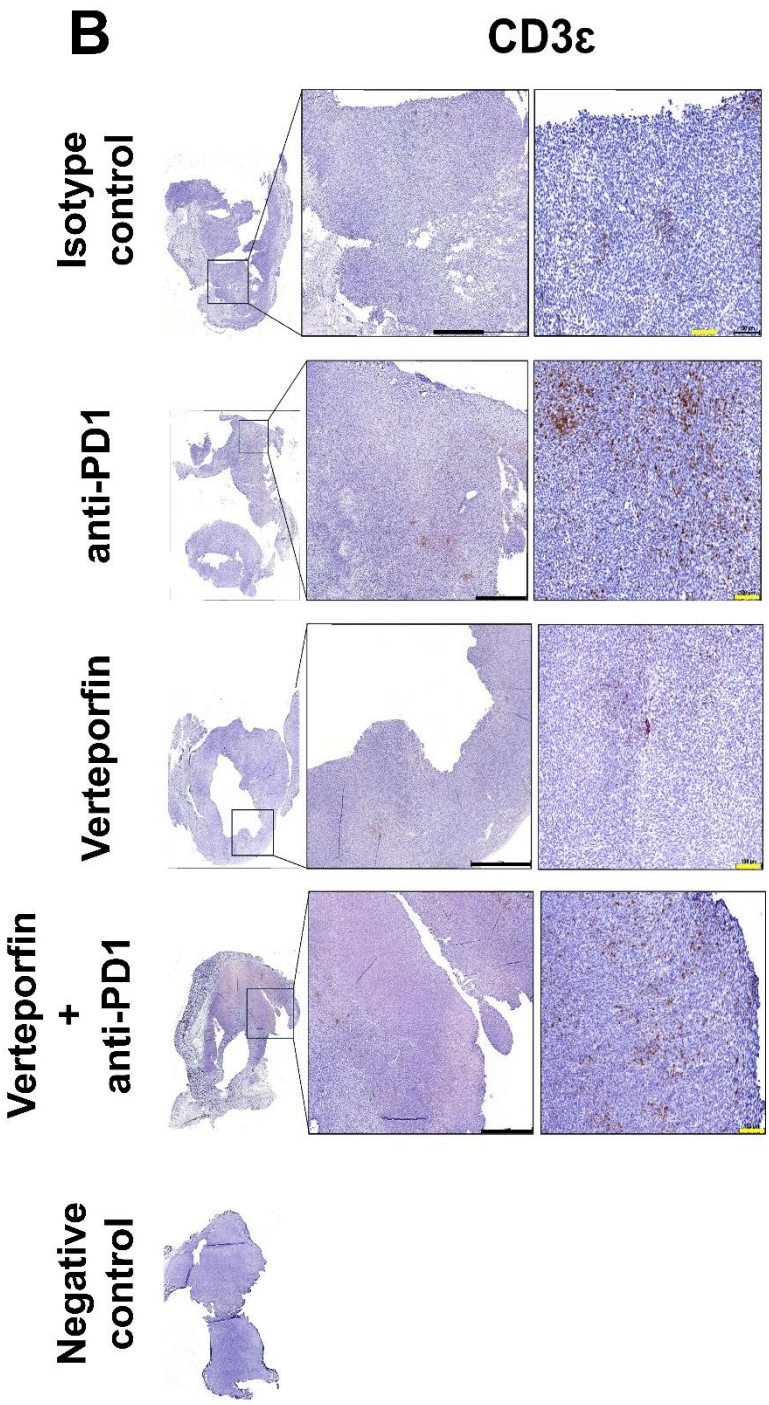

Figure 8. Hematoxylin and eosin staining **(A)**, PCNA **(A)** and CD3ε **(B)** immunohistochemical staining of YUMM1.7 mice tumor samples. Black scale bars on PCNA and CD3ε staining indicate 1000 µm length (*10x magnification*), and the yellow scale bar on CD3ε staining shows 100 µm (*40x magnification*). Negative controls did not contain primary antibodies. Source: (81).

Further investigation of tumor-associated immune cell types revealed overexpression of *PTPRC* (CD45, leukocyte common antigen) in the verteporfin+anti-PD1 group ($p = 0.045$), a pan-leukocyte marker essential for lymphocyte activation. Additionally, verteporfin monotherapy downregulated *FOXP3* (forkhead box protein 3) expression compared to anti-PD1 treatment ($p = 0.031$), with a similar but non-significant trend observed after combination therapy, suggesting that VP may help to counteract immune-suppressive, tumor-promoting signals. In the combination therapy group, *CD68* was elevated ($p = 0.009$ vs. isotype control, $p = 0.029$ vs. anti-PD1), along with *CD86* ($p = 0.026$ vs. isotype control, $p = 0.048$ vs. VP) and *CD80* ($p = 0.030$ vs. anti-PD1), markers typically expressed on pro-inflammatory, tumor-eliminating M1 macrophages (**Figure 9**) (81). *PDCD1* (PD-1) expression increased after anti-PD1 monotherapy and combination therapy compared to VP monotherapy ($p = 0.013$, $p = 0.024$, respectively), while *CD274* (PD-L1) showed no differences across groups (81). Similarly, no significant differences were detected in the immunosuppressive neutrophil marker, *LY6G* (lymphocyte antigen 6 family member G) (81).

These findings indicate that anti-PD1 monotherapy is entirely ineffective in immunologically cold, exhausted tumors like B16-F10 and YUMM17. Despite optimal conditions following anti-PD1 therapy in YUMM.17 tumor – such as the presence of immune cells and high expression of PD-1 and PD-L1 – the therapeutic efficacy was hindered, likely due to YAP1 overactivation (81). Adding verteporfin to checkpoint-arrested, immune-infiltrated, YAP1-overexpressed tumors enhance anti-PD1 therapy by improving immune recognition.

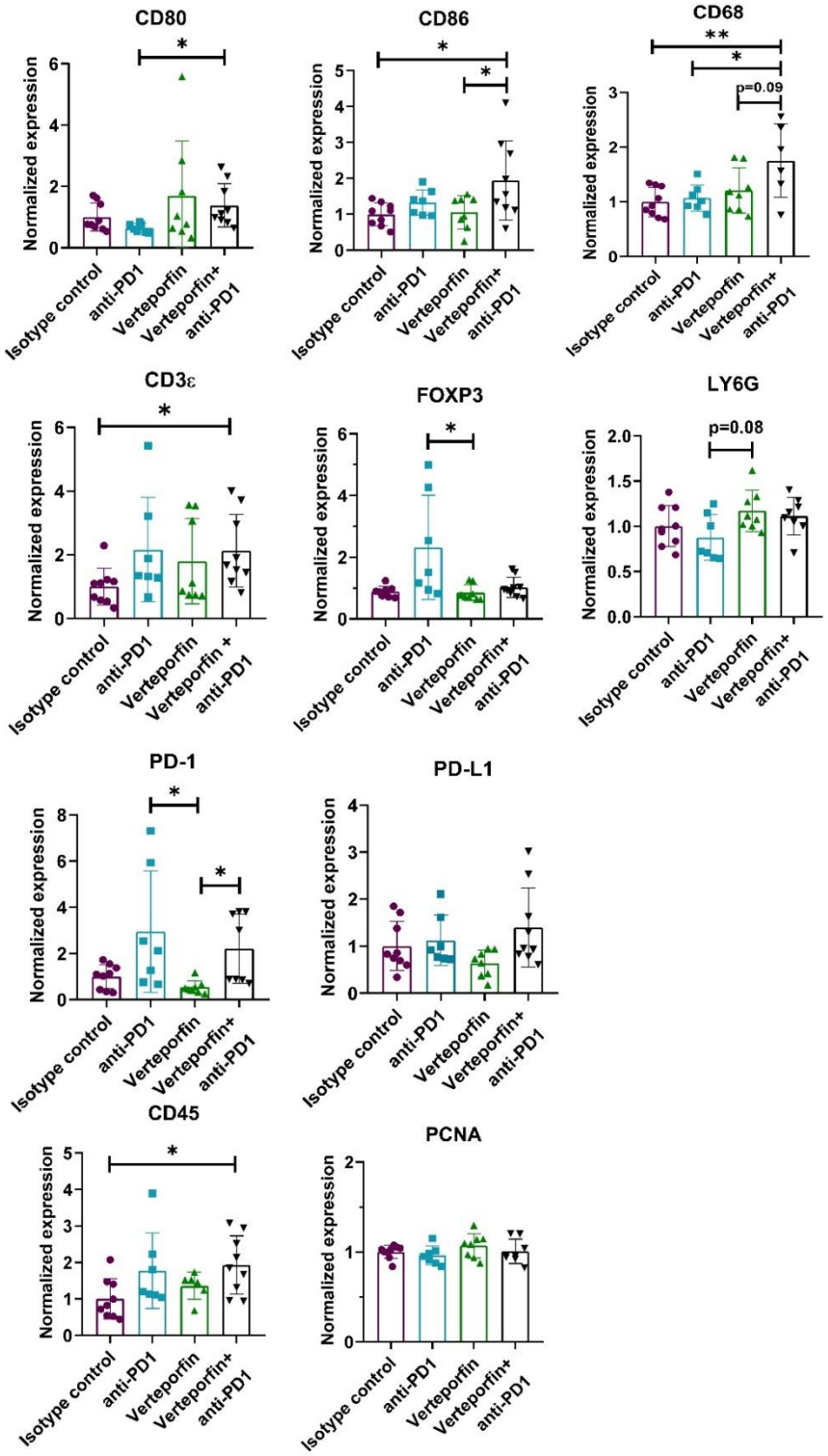

Figure 9. RT-qPCR data of YUMM1.7 tumors are visualized as $2^{-\Delta\Delta Cp}$ values. One-way ANOVA (Tukey's), or Kruskal–Wallis (Dunn's) tests were used for the calculation. The animal numbers used measurements were as follows: isotype control (n = 8-9), anti-PD1 (n = 7), verteporfin (VP) (n = 6-8), VP+anti-PD1 (n = 6-9). *$P \leq 0.05$, **$P \leq 0.01$. Source: (81).

5. DISCUSSION

Our first aim was to set up a transcriptomic and clinical database of cancer patients treated with anti-PD1, anti-PD-L1, and anti-CTLA4 inhibitors. The strength of the integrated platform lies in its use of real-world, high-number patient data. While individual studies often have a limited sample size, our cohort contains 1,434 samples from 19 studies of several tumor types that enhances statistical power and biomarker discovery (6). We integrated our database to ROC Plotter Immunotherapy (www.rocplot.com/immune) and Kaplan-Meier Plotter Immunotherapy (https://www.kmplot.com/analysis/index.php?p=service&cancer=immunotherapy) web services (81). Because of the small sample sizes, we could not identify any druggable biomarkers of anti-PD-L1 resistance. However, it is worth to mention that granzyme H (*GZMH*, AUC = 0.625, p = 1.2E-06, FC = 1.8), and granulysin (*GNLY*, AUC = 0.624, p = 1.4E-06, FC = 1.25) were overexpressed in the responding patients – indicating the activation of NK cells and $CD8^+$ T lymphocytes. In the anti-CTLA-4 resistant cohort though, *BLCAP* – a potential prognostic biomarker (100) – might be worth for further investigations in urothelial and bladder cancer, as aristolochic acid I has been found to interfere with *BLCAP* expression (101).

In the pan-cancer anti-PD1 cohort, there were many promising targets that showed overexpression besides *YAP1*. For example, activation of *FGFR3* has already been connected to low ICI responses in bladder and urothelial cancer (102–104), and many small-molecule inhibitors are available (e.g., anlotinib, infigratinib, pemigatinib) (105,106). *SRC* is another important oncogene with FDA-approved inhibitors (e.g. bosutinib, dasatinib, ponatinib). SRC plays a central role in regulating cell proliferation, survival and immune recognition (107). Venetoclax is currently the only FDA-approved small-molecule inhibitor targeting BCL2 – a key regulator of apoptosis and cell survival (108,109). SETD7 contributes to tumorigenesis in a multiple way e.g. promoting proliferation, activating stem-cell properties, and supporting an immunosuppressive milieu (96). SETD7-targeting drugs, such as DC-S100, cyproheptadine, and (R)-PFI-2, have been investigated with promising results (110–113). SPIN1 plays a role in the epigenetic regulation of oncogenic pathways and is frequently overexpressed in various cancers, with many favourable inhibitors e.g. A366,VinSpinIn (114).

Strangely enough, majority of the mentioned biomarkers has been linked to YAP1 activation. TEAD3 is one of the four transcription factors that upon binding to, YAP1 regulates oncogenic pathways (50). SRC was found to enhance YAP/TAZ activation through LATS repression in an integrin/ actin cytoskeletal manner in melanoma (94). Methylation of YAP1 at K494 by SETD7 drives oncogenic and immunosuppressive Wnt/β-catenin pathway by disrupting the Hippo-signalling (96,115). YAP1 regulates the co-expression of FGFR1 and PD-L1 in lung cancer (116), and controls BCL-2 expression in colorectal cancer (97). STK35, closely related to Hippo pathway participants STK3/4, can enhance chemoresistance through AKT signalling pathways (98)– which is a known activator of YAP1. These results show that YAP1 is a key player in anti-PD1 resistance and warrant further investigations.

The second aim was to investigate YAP1 inhibition to potentiate anti-PD1 efficacy using B16-F10 and YUMM1.7 melanoma cell lines. Verteporfin, a YAP1 inhibitor, reduced cell viability after 24 hours incubation at 5 μM in YUMM1.7, and 10 μM in B16-F10. Longer incubation period (48 hours) enhanced sensitivity to verteporfin, as 1 μM concentration was enough to decrease cell survival in both cell lines.

The combination therapy of verteporfin and anti-PD1 demonstrated the highest efficacy in YUMM1.7-inoculated mice for tumor growth blockade in C57BL/6J mice. However, neither verteporfin, anti-PD1, nor their combination showed therapeutic benefits in B16-F10-inoculated mice. Notably, YUMM1.7 tumors showed more ulceration, aligning with previous findings that melanomas with increased nuclear YAP1 expression are more ulcerative, which is associated with tumor progression, higher invasiveness, and recurrence (117). We observed that the combination of verteporfin and anti-PD1 increased T-cell infiltration, as indicated by the upregulation of *CD3ε* and *PTPRC* (CD45) markers in YUMM1.7 tumors – overcoming the otherwise immune-exhausted profile, which is characterized by impaired lymphocyte infiltration and activation (82). This suggests that verteporfin may help reverse immune-poor conditions by promoting lymphocyte infiltration. These positive effects are likely due to the higher YAP1 expression in YUMM1.7 tumors compared to B16-F10, making them more susceptible to verteporfin. Genetic differences between the two cell lines influenced treatment responses as YUMM1.7 carries $BRAF^{V600E}$, *PTEN*, and *CDKN2A* mutations (118), whereas B16-F10 is wild-type for *BRAF* (83, 119). Given the interplay between

the RAS/MAPK,- and Hippo-pathways, *BRAF*-mutated tumors like YUMM1.7 can be more dependent on YAP1 activation for immune evasion, whereas B16-F10 tumors are likely less reliant on YAP1 for survival. Despite *YAP1* expression is not directly affected by anti-PD1 therapy in our tumor models, studies show that *YAP1* contributes to anti-PD1 resistance by promoting an immunosuppressive tumor microenvironment (120,121) and immune evasion in melanoma (122).

Our findings suggest that YUMM1.7 tumors, due to their activated MAPK-pathway, might be more dependent on immune regulation, since verteporfin primarily increased T-cell and macrophage markers without significantly reducing tumor proliferation. The antitumor activity of Verteporfin seems to be driven more by immune modulation than by direct cytotoxicity, which, while observable, does not appear to be the dominant mechanism – highlighting its potential as an effective combination partner for anti-PD1 therapy. In contrast, B16-F10 tumors may rely more on unchecked proliferation rather than immune evasion, rendering them resistant to immune-based treatments.

Verteporfin has been shown to reduce PD-L1 expression by targeting YAP1 in melanoma (87). Consistently, our findings demonstrated the greatest reduction in *PDCD1* (PD-1) and *CD274* (PD-L1) expression in the VP-treated group (81). Apart from regulating the PD-1/PD-L1 axis, YAP1 also influences immune cell recruitment, as seen by the increased expression of *CD68*, *CD80*, and *CD86*, indicating enhanced M1 macrophage infiltration after combination therapy. As shown by others, YUMM1.7 tumors exhibit lower intratumoral IFN-γ levels, which is notable since these cytokines play a key role in macrophage differentiation and activation (123). Furthermore, by using the established ICI database, we identified IFN-γ-related gene expression signatures associated with anti-PD1 therapy responses in melanoma (124). Eleven differentially expressed genes associated with *in vitro*-acquired IFN resistance were also altered in our *in silico* cohort of patients treated with immune checkpoint inhibitors (124). Among these, the following were interferon-regulated genes: *SOX4* (FC = 2.23 in non-responders, p = 1.57E-11), *DEK* (FC = 1.41 in non-responders, p = 1.66E-06), and *HSPA1B* (FC = 1.75 in responders, p = 2.96E-04). Additionally, we found that *in vivo*-identified IFN-resistance genes *CDCA4* (FC = 2.05, p = 5.90E-09) and *AQP1* (FC = 2.06, p = 2.13E-06), were also overexpressed in ICI-resistant samples, reinforcing their potential role in

therapy resistance. Interestingly, IFN-resistance genes were also differentially expressed in melanoma brain and lung metastases and were linked to reduced anti-PD1 efficacy (125). The relationship between IFN and ICI treatment efficacy has also been highlighted by others, as IFN-γ has been associated with increased PD-L1 expression, YAP1 activation, and anti-PD1 resistance (126,127).

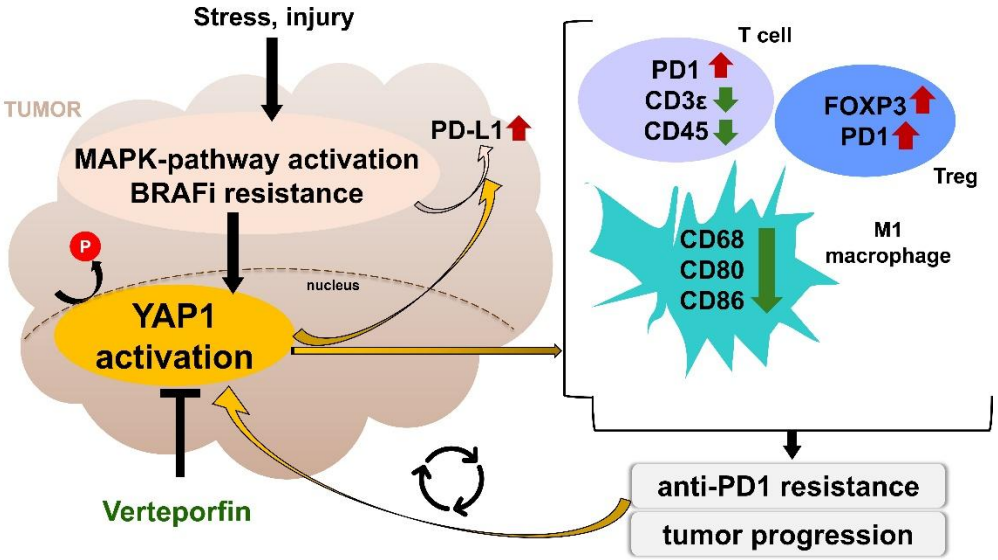

Figure 10. Summary of the interplay between MAPK-pathway (*RAS, BRAF, CRAF, MAP4K*), Hippo-pathway (*YAP1*), and PD-1-pathway.

In summary, verteporfin plus anti-PD1 promotes a pro-inflammatory tumor microenvironment by enhancing T-cell and M1 macrophage infiltration, highlighting the potential of this combination therapy in (*BRAF*-mutant) melanoma (**Figure 10**).

6. CONCLUSIONS

1. **Robust database of immune checkpoint inhibitor-treated cancer patients**
    a. We set up a comprehensive database by compiling datasets from the NCBI GEO, Cancer Research Institute iAtlas, and literature sources.
    b. Nineteen datasets from solid tumors, collected before or after treatment with nivolumab, pembrolizumab, atezolizumab, durvalumab, or ipilimumab, were included in the final version.
    c. A total of 1,434 tumor tissue samples from 1,323 patients, along with corresponding clinical characteristics, survival data, and transcriptomic data, were integrated into ROC Plotter Immunotherapy and Kaplan-Meier Plotter Immunotherapy web platforms.
2. **Predictive, tumor-agnostic biomarkers of immune checkpoint inhibitor resistance**
    a. We identified predictive markers of baseline resistance to immune checkpoint inhibitors in the following cohorts:
    b. Anti-PD1 pre-treatment group: 29,755 genes screened, 912 remained significant after multiple hypothesis testing. *YAP1*, and its regulator molecules, *TEAD3*, *SRC*, *SETD7*, *FGFR3*, *BCL2*, *STK35* were overexpressed in non-responder patients.
    c. Anti-PD-L1 pre-treatment group: 26,819 genes analyzed, 38 significant, but no upregulated, druggable resistance marker was found.
    d. Anti-CTLA-4 pre-treatment group: 22,561 genes analyzed, 80 significant markers, with *BLCAP* emerging as a potential druggable target.
3. **YAP1 as a druggable biomarker of anti-PD1 resistance in melanoma**
    a. Since melanoma was the most represented cancer type in the database, we focused on the anti-PD1 pre-treatment group (n = 415) only. We identified *YAP1* as the strongest predictive and prognostic biomarker, associated with therapy resistance (ROC AUC = 0.699, FC = 1.8, p = 1.1E-08), and poorer survival outcomes (PFS: HR = 2.51, p = 1.2E-06, FDR = 1%, and OS: HR = 2.15, p = 1.2E-05, FDR = 1%).
    b. We chose YAP1 for *in vivo* validation with the utilization of a clinically available inhibitor, verteporfin.

4. **Targeting YAP1 with verteporfin to overcome anti-PD1 resistance**
    a. We demonstrated that verteporfin significantly reduced tumor cell viability in a dose,- and time-dependent manner in B16-F10 and YUMM1.7 melanoma cell lines. YUMM1.7 cells were more sensitive to VP treatment than B16-F10 cells.
    b. In C57BL/6J mice with $BRAF^{V600E}$ YUMM1.7 tumors, the combination of verteporfin and anti-PD1 therapy resulted in the greatest reduction in tumor size and weight, significantly outperforming anti-PD1 monotherapy. Wild-type B16-F10 tumors, which exhibited lower *YAP1* expression both before and after treatment, remained unresponsive to all treatments.
    c. Tumors with $BRAF^{V600E}$ might be linked to increased *YAP1* expression, making them more susceptible to verteporfin.
    d. B16-F10 tumors, lacking *YAP1* overexpression and high mutational frequency, were unresponsive to anti-PD1 or verteporfin, underscoring the specificity of YAP1-driven resistance.
    e. We confirmed that *YAP1* overexpression is a major driver of anti-PD1 resistance in melanoma.
5. **Immune modulation by verteporfin: from cold tumors to hot tumors**
    a. RT-qPCR and immunostaining of YUMM1.7 tumors showed that verteporfin+anti-PD1 therapy enhanced immune infiltration, shifting tumors from an immune-excluded ("cold") phenotype to a more infiltrated state.
    b. The combination therapy increased *CD3ε*, *PTPRC* (CD45) levels, showing activation of lymphocytes.
    c. It decreased *FOXP3* levels, suggesting reduced activation of immunosuppressive regulatory T cells.
    d. *CD68*, *CD80*, and *CD86* – pro-inflammatory M1 macrophage markers – were increased following verteporfin+anti-PD1 treatment, suggesting activation anti-tumoral immune response.
    e. No significant differences were observed in *CD274* (PD-L1) or *LY6G* expression.

7. SUMMARY

We established a comprehensive and integrative database of cancer patients treated with anti-PD1, anti-PD-L1, and anti-CTLA-4 immune checkpoint inhibitors. The final version includes 1,434 tumor tissue samples collected before or after treatment, along with clinical survival data and transcriptomic profiles, all integrated into a web platform (www.rocplot.com/immune). This database has proven to be a valuable tool for identifying novel biomarkers of ICI resistance and potential therapeutic targets.

Through an extensive analysis, we found that *YAP1* and its regulatory partners – *TEAD3*, *SRC*, *SETD7*, *FGFR3*, *BCL2*, and *STK35* – were overexpressed in the anti-PD1 resistant patients. Further analysis provided strong evidence that *YAP1* is a key biomarker and a potential therapeutic target in anti-PD1-resistant melanoma. Consequently, we selected *YAP1* for *in vitro*, and *in vivo* validation using verteporfin, a clinically available inhibitor. Experiments in melanoma cell lines demonstrated that verteporfin significantly reduced tumor cell viability, with YUMM1.7 cells exhibiting slightly higher sensitivity than B16-F10 cells. This trend was also observed *in vivo*, where YUMM1.7-bearing mice showed the greatest tumor reduction when treated with the combination of verteporfin and anti-PD1, outperforming both monotherapies. In contrast, B16-F10 tumors remained unresponsive to all treatments, correlating with their lower YAP1 expression. These findings underscore the specificity of *YAP1*-driven ICI resistance, particularly in $BRAF^{V600E}$ tumors. By investigation of the dissected tumors, verteporfin was found to modulate the immune landscape, shifting immune-excluded ("cold") tumors into a more immune-infiltrated ("hot") phenotype. This was evidenced by increased *CD3ε* and *PTPRC* (CD45) expression (indicating enhanced lymphocyte activation), by reduced *FOXP3* levels (suggesting lower immunosuppressive signals by regulatory T cells), and by elevated *CD68*, *CD80*, and *CD86* expression (showing pro-inflammatory M1 macrophage-driven anti-tumoral responses). Notably, *CD274* (PD-L1) and *LY6G* expression remained unchanged across treatment groups. Our findings highlight YAP1 inhibition as a promising strategy for overcoming anti-PD1 resistance, particularly in *BRAF*-mutant, *YAP1*-overexpressing melanomas.

Our validated database serves as a high-quality resource for ongoing and future research, facilitating discoveries that can refine therapeutic approaches and improve patient outcomes.

8. REFERENCES

1. Siegel RL, Kratzer TB, Giaquinto AN, Sung H, Jemal A. Cancer statistics, 2025. CA: A Cancer Journal for Clinicians. 2025;75(1):10–45.

2. Aaltonen LA, Abascal F, Abeshouse A, Aburatani H, Adams DJ, Agrawal N, et al. Pan-cancer analysis of whole genomes. Nature. 2020 Feb;578(7793):82–93.

3. Herms A, Jones PH. Somatic Mutations in Normal Tissues: New Perspectives on Early Carcinogenesis. Annual Review of Cancer Biology. 2023 Apr 11;7(Volume 7, 2023):189–205.

4. Zhang S, Xiao X, Yi Y, Wang X, Zhu L, Shen Y, Lin D, Wu C. Tumor initiation and early tumorigenesis: molecular mechanisms and interventional targets. Sig Transduct Target Ther. 2024 Jun 19;9(1):1–36.

5. Hanahan D. Hallmarks of Cancer: New Dimensions. Cancer Discovery. 2022 Jan 12;12(1):31–46.

6. Kovács SA, Fekete JT, Győrffy B. Predictive biomarkers of immunotherapy response with pharmacological applications in solid tumors. Acta Pharmacol Sin. 2023 Sep;44(9):1879–89.

7. Hodi FS, O'Day SJ, McDermott DF, Weber RW, Sosman JA, Haanen JB, Gonzalez R, Robert C, Schadendorf D, Hassel JC, Akerley W, van den Eertwegh AJM, Lutzky J, Lorigan P, Vaubel JM, Linette GP, Hogg D, Ottensmeier CH, Lebbé C, Peschel C, Quirt I, Clark JI, Wolchok JD, Weber JS, Tian J, Yellin MJ, Nichol GM, Hoos A, Urba WJ. Improved survival with ipilimumab in patients with metastatic melanoma. N Engl J Med. 2010 Aug 19;363(8):711–23.

8. Motzer RJ, Tannir NM, McDermott DF, Arén Frontera O, Melichar B, Choueiri TK, Plimack ER, Barthélémy P, Porta C, George S, Powles T, Donskov F, Neiman V, Kollmannsberger CK, Salman P, Gurney H, Hawkins R, Ravaud A, Grimm MO, Bracarda S, Barrios CH, Tomita Y, Castellano D, Rini BI, Chen AC, Mekan S, McHenry MB, Wind-Rotolo M, Doan J, Sharma P, Hammers HJ, Escudier B,

CheckMate 214 Investigators. Nivolumab plus Ipilimumab versus Sunitinib in Advanced Renal-Cell Carcinoma. N Engl J Med. 2018 Apr 5;378(14):1277–90.

9. Hammers HJ, Plimack ER, Infante JR, Rini BI, McDermott DF, Lewis LD, Voss MH, Sharma P, Pal SK, Razak ARA, Kollmannsberger C, Heng DYC, Spratlin J, McHenry MB, Amin A. Safety and Efficacy of Nivolumab in Combination With Ipilimumab in Metastatic Renal Cell Carcinoma: The CheckMate 016 Study. J Clin Oncol. 2017;35(34):3851–8.

10. Overman MJ, Lonardi S, Wong KYM, Lenz HJ, Gelsomino F, Aglietta M, Morse MA, Van Cutsem E, McDermott R, Hill A, Sawyer MB, Hendlisz A, Neyns B, Svrcek M, Moss RA, Ledeine JM, Cao ZA, Kamble S, Kopetz S, André T. Durable Clinical Benefit With Nivolumab Plus Ipilimumab in DNA Mismatch Repair-Deficient/Microsatellite Instability-High Metastatic Colorectal Cancer. J Clin Oncol. 2018 Mar 10;36(8):773–9.

11. Yau T, Kang YK, Kim TY, El-Khoueiry AB, Santoro A, Sangro B, Melero I, Kudo M, Hou MM, Matila A, Tovoli F, Knox JJ, Ruth He A, El-Rayes BF, Acosta-Rivera M, Lim HY, Neely J, Shen Y, Wisniewski T, Anderson J, Hsu C. Efficacy and Safety of Nivolumab Plus Ipilimumab in Patients With Advanced Hepatocellular Carcinoma Previously Treated With Sorafenib. JAMA Oncol. 2020 Nov;6(11):e204564.

12. Hellmann MD, Paz-Ares L, Bernabe Caro R, Zurawski B, Kim SW, Carcereny Costa E, Park K, Alexandru A, Lupinacci L, de la Mora Jimenez E, Sakai H, Albert I, Vergnenegre A, Peters S, Syrigos K, Barlesi F, Reck M, Borghaei H, Brahmer JR, O'Byrne KJ, Geese WJ, Bhagavatheeswaran P, Rabindran SK, Kasinathan RS, Nathan FE, Ramalingam SS. Nivolumab plus Ipilimumab in Advanced Non-Small-Cell Lung Cancer. N Engl J Med. 2019 Nov 21;381(21):2020–31.

13. Paz-Ares L, Ciuleanu TE, Cobo M, Schenker M, Zurawski B, Menezes J, Richardet E, Bennouna J, Felip E, Juan-Vidal O, Alexandu A, Sakai H, Lingua A, Salman P, Souquet PJ, De Marchi P, Martin C, Pérol M, Scherpereel A, Lu S, John T, Carbone DP, Meadows-Shropshire S, Agrawal S, Oukessou A, Yan J, Reck M. First-line nivolumab plus ipilimumab combined with two cycles of chemotherapy in patients

with non-small-cell lung cancer (CheckMate 9LA): an international, randomised, open-label, phase 3 trial. Lancet Oncol. 2021 Feb;22(2):198–211.

14. Baas P, Scherpereel A, Nowak AK, Fujimoto N, Peters S, Tsao AS, Mansfield AS, Popat S, Jahan T, Antonia S, Oulkhouir Y, Bautista Y, Cornelissen R, Greillier L, Grossi F, Kowalsi D, Rodríguez-Cid J, Aanur P, Oukessou A, Baudelet C, Zalcman G. First-line nivolumab plus ipilimumab in unresectable malignant pleural mesothelioma (CheckMate 743): a multicentre, randomised, open-label, phase 3 trial. Lancet. 2021 Jan 30;397(10272):375–86.

15. Kovács SA, Győrffy B. Transcriptomic datasets of cancer patients treated with immune-checkpoint inhibitors: a systematic review. J Transl Med. 2022 May 31;20(1):249.

16. Wei J, Li W, Zhang P, Guo F, Liu M. Current trends in sensitizing immune checkpoint inhibitors for cancer treatment. Molecular Cancer. 2024 Dec 26;23(1):279.

17. Baumeister SH, Freeman GJ, Dranoff G, Sharpe AH. Coinhibitory Pathways in Immunotherapy for Cancer. Annu Rev Immunol. 2016 May 20;34:539–73.

18. Sun C, Mezzadra R, Schumacher TN. Regulation and Function of the PD-L1 Checkpoint. Immunity. 2018 Mar 20;48(3):434–52.

19. Hamid O, Robert C, Daud A, Hodi FS, Hwu WJ, Kefford R, Wolchok JD, Hersey P, Joseph R, Weber JS, Dronca R, Mitchell TC, Patnaik A, Zarour HM, Joshoua AM, Zhao Q, Jensen E, Ahsan S, Ibrahim N, Ribas A. Five-year survival outcomes for patients with advanced melanoma treated with pembrolizumab in KEYNOTE-001. Ann Oncol. 2019 Apr 1;30(4):582–8.

20. Hui R, Garon EB, Goldman JW, Leighl NB, Hellmann MD, Patnaik A, Gandhi L, Eder JP, Ahn MJ, Horn L, Felip E, Carcereny E, Rangwala R, Lubiniecki GM, Zhang J, Emancipator K, Roach C, Rizvi NA. Pembrolizumab as first-line therapy for patients with PD-L1-positive advanced non-small cell lung cancer: a phase 1 trial. Ann Oncol. 2017 Apr 1;28(4):874–81.

21. Cortes J, Cescon DW, Rugo HS, Nowecki Z, Im SA, Yusof MM, Gallardo C, Lipatov O, Barrios CH, Holgado E, Iwata H, Masuda N, Otero MT, Gokmen E, Loi S, Guo Z, Zhao J, Aktan G, Karantza V, Schmid P, KEYNOTE-355 Investigators. Pembrolizumab plus chemotherapy versus placebo plus chemotherapy for previously untreated locally recurrent inoperable or metastatic triple-negative breast cancer (KEYNOTE-355): a randomised, placebo-controlled, double-blind, phase 3 clinical trial. Lancet. 2020;396(10265):1817–28.

22. Borcoman E, Le Tourneau C. Keynote-158 study, FDA granted accelerated approval of pembrolizumab for the treatment of patients with advanced PD-L1-positive cervical cancer. Ann Transl Med. 2020 Dec;8(23):1611.

23. Balar AV, Castellano D, O'Donnell PH, Grivas P, Vuky J, Powles T, Plimack ER, Hahn NM, de Wit R, Pang L, Savage MJ, Perini RF, Keefe SP, Bajorin D, Bellmunt J. First-line pembrolizumab in cisplatin-ineligible patients with locally advanced and unresectable or metastatic urothelial cancer (KEYNOTE-052): a multicentre, single-arm, phase 2 study. Lancet Oncol. 2017 Nov;18(11):1483–92.

24. Cohen EEW, Soulières D, Le Tourneau C, Dinis J, Licitra L, Ahn MJ, Soria A, Machiels JP, Mach N, Mehra R, Burtness B, Zhang P, Cheng J, Swaby RF, Harrington KJ, KEYNOTE-040 investigators. Pembrolizumab versus methotrexate, docetaxel, or cetuximab for recurrent or metastatic head-and-neck squamous cell carcinoma (KEYNOTE-040): a randomised, open-label, phase 3 study. Lancet. 2019 Jan 12;393(10167):156–67.

25. Shah MA, Kojima T, Hochhauser D, Enzinger P, Raimbourg J, Hollebecque A, Lordick F, Kim SB, Tajika M, Kim HT, Lockhart AC, Arkenau HT, El-Hajbi F, Gupta M, Pfeiffer P, Liu Q, Lunceford J, Kang SP, Bhagia P, Kato K. Efficacy and Safety of Pembrolizumab for Heavily Pretreated Patients With Advanced, Metastatic Adenocarcinoma or Squamous Cell Carcinoma of the Esophagus: The Phase 2 KEYNOTE-180 Study. JAMA Oncology. 2019 Apr 1;5(4):546–50.

26. Bang YJ, Kang YK, Catenacci DV, Muro K, Fuchs CS, Geva R, Hara H, Golan T, Garrido M, Jalal SI, Borg C, Doi T, Yoon HH, Savage MJ, Wang J, Dalal RP, Shah

S, Wainberg ZA, Chung HC. Pembrolizumab alone or in combination with chemotherapy as first-line therapy for patients with advanced gastric or gastroesophageal junction adenocarcinoma: results from the phase II nonrandomized KEYNOTE-059 study. Gastric Cancer. 2019 Jul;22(4):828–37.

27. Marabelle A, Fakih M, Lopez J, Shah M, Shapira-Frommer R, Nakagawa K, Chung HC, Kindler HL, Lopez-Martin JA, Miller WH, Italiano A, Kao S, Piha-Paul SA, Delord JP, McWilliams RR, Fabrizio DA, Aurora-Garg D, Xu L, Jin F, Norwood K, Bang YJ. Association of tumour mutational burden with outcomes in patients with advanced solid tumours treated with pembrolizumab: prospective biomarker analysis of the multicohort, open-label, phase 2 KEYNOTE-158 study. Lancet Oncol. 2020 Oct;21(10):1353–65.

28. Marcus L, Lemery SJ, Keegan P, Pazdur R. FDA Approval Summary: Pembrolizumab for the Treatment of Microsatellite Instability-High Solid Tumors. Clin Cancer Res. 2019 Jul 1;25(13):3753–8.

29. Pophali P, Varela JC, Rosenblatt J. Immune checkpoint blockade in hematological malignancies: current state and future potential. Front Oncol. 2024;14:1323914.

30. Larkin J, Minor D, D'Angelo S, Neyns B, Smylie M, Miller WH, Gutzmer R, Linette G, Chmielowski B, Lao CD, Lorigan P, Grossmann K, Hassel JC, Sznol M, Daud A, Sosman J, Khushalani N, Schadendorf D, Hoeller C, Walker D, Kong G, Horak C, Weber J. Overall Survival in Patients With Advanced Melanoma Who Received Nivolumab Versus Investigator's Choice Chemotherapy in CheckMate 037: A Randomized, Controlled, Open-Label Phase III Trial. J Clin Oncol. 2018 Feb 1;36(4):383–90.

31. Kato K, Cho BC, Takahashi M, Okada M, Lin CY, Chin K, Kadowaki S, Ahn MJ, Hamamoto Y, Doki Y, Yen CC, Kubota Y, Kim SB, Hsu CH, Holtvhed E, Xynos I, Kodani M, Kitagawa Y. Nivolumab versus chemotherapy in patients with advanced oesophageal squamous cell carcinoma refractory or intolerant to previous chemotherapy (ATTRACTION-3): a multicentre, randomised, open-label, phase 3 trial. Lancet Oncol. 2019;20(11):1506–17.

32. Mankor JM, Disselhorst MJ, Poncin M, Baas P, Aerts JGJV, Vroman H. Efficacy of nivolumab and ipilimumab in patients with malignant pleural mesothelioma is related to a subtype of effector memory cytotoxic T cells: Translational evidence from two clinical trials. EBioMedicine. 2020;62:103040.

33. Twomey JD, Zhang B. Cancer Immunotherapy Update: FDA-Approved Checkpoint Inhibitors and Companion Diagnostics. AAPS J. 2021 Mar 7;23(2):39.

34. Gupta AK, Mann A, Vincent K, Abramovits W. Libtayo® (Cemiplimab-rwlc) Injection for Intravenous Use. Skinmed. 2024;22(2):138–43.

35. Makharadze T, Gogishvili M, Melkadze T, Baramidze A, Giorgadze D, Penkov K, Laktionov K, Nemsadze G, Nechaeva M, Rozhkova I, Kalinka E, Li S, Li Y, Kaul M, Quek RGW, Pouliot JF, Seebach F, Lowy I, Gullo G, Rietschel P. Cemiplimab Plus Chemotherapy Versus Chemotherapy Alone in Advanced NSCLC: 2-Year Follow-Up From the Phase 3 EMPOWER-Lung 3 Part 2 Trial. J Thorac Oncol. 2023 Jun;18(6):755–68.

36. Rosenberg JE, Hoffman-Censits J, Powles T, van der Heijden MS, Balar AV, Necchi A, Dawson N, O'Donnell PH, Balmanoukian A, Loriot Y, Srinivas S, Retz MM, Grivas P, Josep RW, Galsky MD, Fleming MT, Petrylak DP, Perez-Gracia JL, Burris HA, Castellano D, Canil C, Bellmunt J, Bajorin D, Nickles D, Bourgon R, Frampton Garret M, Cui N, Mariathasan S, Abidoye O, Fine GD, Dreicher R. Atezolizumab in patients with locally advanced and metastatic urothelial carcinoma who have progressed following treatment with platinum-based chemotherapy: a single-arm, multicentre, phase 2 trial. Lancet. 2016 May 7;387(10031):1909–20.

37. Chen AP, Sharon E, O'Sullivan-Coyne G, Moore N, Foster JC, Hu JS, Van Time BA, Conley AP, Read WL, Riedel RF, Burgess MA, Glod J, David EJ, Merriam P, Naqash AR, Fino KK, Miller BL, Wilsker DF, Begum A, Ferry-Galow KV, Deshpande HA, Schwartz GK, Ladle BH, Okuno SH, Beck JC, Chen JL, Takebe N, Fogli LK, Rosenberger CL, Parchment RE, Doroshow JH. Atezolizumab for Advanced Alveolar Soft Part Sarcoma. N Engl J Med. 2023 Sep 7;389(10):911–21.

38. Walker JW, Lebbé C, Grignani G, Nathan P, Dirix L, Fenig E, Ascierto PA, Sandhu S, Munhoz R, Benincasa E, Flaskett S, Reed J, Engelsberg A, Hariharan S, Kasturi V. Efficacy and safety of avelumab treatment in patients with metastatic Merkel cell carcinoma: experience from a global expanded access program. J Immunother Cancer. 2020 Apr;8(1):e000313.

39. Apolo AB, Ellerton JA, Infante JR, Agrawal M, Gordon MS, Aljumaily R, Gourdin T, Dirix L, Lee KW, Taylor MH, Schöffski P, Wang D, Ravaud A, Manitz J, Pennock G, Ruisi M, Gulley JL, Patel MR. Avelumab as second-line therapy for metastatic, platinum-treated urothelial carcinoma in the phase Ib JAVELIN Solid Tumor study: 2-year updated efficacy and safety analysis. J Immunother Cancer. 2020 Oct;8(2):e001246.

40. Sangro B, Chan SL, Kelley RK, Lau G, Kudo M, Sukeepaisarnjaroen W, Yarchoan M, Toni END, Furuse J, Kang YK, Galle PR, Rimassa L, Heurgué A, Tam VC, Dao TV, Thungappa SC, Breder V, Ostapenko Y, Reig M, Makowsky M, Paskow MJ, Gupta C, Kurland JF, Negro A, Abou-Alfa GK, HIMALAYA investigators. Four-year overall survival update from the phase III HIMALAYA study of tremelimumab plus durvalumab in unresectable hepatocellular carcinoma. Annals of Oncology. 2024 May 1;35(5):448–57.

41. Paz-Ares L, Dvorkin M, Chen Y, Reinmuth N, Hotta K, Trukhin D, Statsenko G, Hochmair MJ, Özgüroğlu M, Ji JH, Voitko O, Poltoratskiy A, Ponce S, Verderame F, Havel L, Bondarenko I, Kazarnowicz A, Losonczy Gy, Conev NV, Armstrong J, Byrne N, Shire N, Jiang H, Goldman JW, CASPIAN investigators. Durvalumab plus platinum-etoposide versus platinum-etoposide in first-line treatment of extensive-stage small-cell lung cancer (CASPIAN): a randomised, controlled, open-label, phase 3 trial. Lancet. 2019 Nov 23;394(10212):1929–39.

42. Fung S, Syed YY. Durvalumab: A Review in Advanced Biliary Tract Cancer. Target Oncol. 2023;18(6):965–72.

43. Westin SN, Moore K, Chon HS, Lee JY, Thomes Pepin J, Sundborg M, Shai A, de la Garza J, Nishio S, Gold MA, Wang K, McIntyre K, Tillmanns TD, Blank SV, Liu

JH, McCollum M, Contreras Mejia F, Nishikawa T, Pennington K, Novak Z, De Melo AC, Sehouli J, Klasa-Mazurkiewicz D, Papadimitriou C, Gil-Martin M, Brasiuniene B, Donnelly C, del Rosario PM, Liu X, Van Nieuwenhuysen E, on behalf of the DUO-E Investigators. Durvalumab Plus Carboplatin/Paclitaxel Followed by Maintenance Durvalumab With or Without Olaparib as First-Line Treatment for Advanced Endometrial Cancer: The Phase III DUO-E Trial. JCO. 2024 Jan 20;42(3):283–99.

44. Ruffo E, Wu RC, Bruno TC, Workman CJ, Vignali DAA. Lymphocyte-activation gene 3 (LAG3): The next immune checkpoint receptor. Semin Immunol. 2019 Apr;42:101305.

45. Anderson NM, Simon MC. Tumor Microenvironment. Curr Biol. 2020 Aug 17;30(16):R921–5.

46. Wu B, Zhang B, Li B, Wu H, Jiang M. Cold and hot tumors: from molecular mechanisms to targeted therapy. Sig Transduct Target Ther. 2024 Oct 18;9(1):1–65.

47. Das S, Johnson DB. Immune-related adverse events and anti-tumor efficacy of immune checkpoint inhibitors. Journal for ImmunoTherapy of Cancer. 2019 Nov 15;7(1):306.

48. Lim SY, Shklovskaya E, Lee JH, Pedersen B, Stewart A, Ming Z, Irvine M, Shivalingam B, Saw RPM, Menzies AM, Carlino MS, Scolyer RA, Long GV, Rizos H. The molecular and functional landscape of resistance to immune checkpoint blockade in melanoma. Nat Commun. 2023 Mar 18;14(1):1516.

49. Vesely MD, Zhang T, Chen L. Resistance Mechanisms to Anti-PD Cancer Immunotherapy. Annu Rev Immunol. 2022 Apr 26;40:45–74.

50. Cunningham R, Hansen CG. The Hippo pathway in cancer: YAP/TAZ and TEAD as therapeutic targets in cancer. Clin Sci (Lond). 2022 Feb;136(3):197–222.

51. Szulzewsky F, Holland EC, Vasioukhin V. YAP1 and its fusion proteins in cancer initiation, progression and therapeutic resistance. Dev Biol. 2021 Jul;475:205–21.

52. Feng R, Gong J, Wu L, Wang L, Zhang B, Liang G, Zheng H, Xiao H. MAPK and Hippo signaling pathways crosstalk via the RAF-1/MST-2 interaction in malignant melanoma. Oncology Reports. 2017 Aug 1;38(2):1199–205.

53. Howard A, Bojko J, Flynn B, Bowen S, Jungwirth U, Walko G. Targeting the Hippo/YAP/TAZ signalling pathway: Novel opportunities for therapeutic interventions into skin cancers. Experimental Dermatology. 2022;31(10):1477–99.

54. Yong J, Li Y, Lin S, Wang Z, Xu Y. Inhibitors Targeting YAP in Gastric Cancer: Current Status and Future Perspectives. Drug Des Devel Ther. 2021 Jun 9;15:2445–56.

55. Mellish KJ, Brown SB. Verteporfin: a milestone in opthalmology and photodynamic therapy. Expert Opinion on Pharmacotherapy. 2001 Feb 1;2(2):351–61.

56. Gibault F, Corvaisier M, Bailly F, Huet G, Melnyk P, Cotelle P. Non-Photoinduced Biological Properties of Verteporfin. Current Medicinal Chemistry. 23(11):1171–84.

57. Liu-Chittenden Y, Huang B, Shim JS, Chen Q, Lee SJ, Anders RA, Liu JO, Pan D. Genetic and pharmacological disruption of the TEAD–YAP complex suppresses the oncogenic activity of YAP. Genes Dev. 2012 Jun 15;26(12):1300–5.

58. Yu FX, Luo J, Mo JS, Liu G, Kim YC, Meng Z, Zhao L, Peyman G, Ouyang H, Jiang W, Zhao J, Chen X, Zhang L, Wang CY, Bastian BC, Zhang K Guan KL. Mutant Gq/11 Promote Uveal Melanoma Tumorigenesis by Activating YAP. Cancer Cell. 2014 Jun 16;25(6):822–30.

59. Wei C, Li X. The Role of Photoactivated and Non-Photoactivated Verteporfin on Tumor. Front Pharmacol. 2020;11:557429.

60. Andrade D, Mehta M, Griffith J, Panneerselvam J, Srivastava A, Kim TD, Janknecht R, Herman T, Ramesh R, Munshi A. YAP1 inhibition radiosensitizes triple negative breast cancer cells by targeting the DNA damage response and cell survival pathways. Oncotarget. 2017;8(58):98495–508.

61. Donohue E, Thomas A, Maurer N, Manisali I, Zeisser-Labouebe M, Zisman N, Anderson HJ, Ng SSW, Webb M, Bally M, Roberge M. The Autophagy Inhibitor Verteporfin Moderately Enhances the Antitumor Activity of Gemcitabine in a Pancreatic Ductal Adenocarcinoma Model. J Cancer. 2013 Aug 28;4(7):585–96.

62. Fu J, McGrath NA, Lee J, Wang X, Brar G, Xie C. Verteporfin synergizes the efficacy of anti-PD-1 in cholangiocarcinoma. Hepatobiliary Pancreat Dis Int. 2022 Oct;21(5):485–92.

63. Maher NG, Vergara IA, Long GV, Scolyer RA. Prognostic and predictive biomarkers in melanoma. Pathology. 2024 Mar;56(2):259–73.

64. Tímár J, Ladányi A. Molecular Pathology of Skin Melanoma: Epidemiology, Differential Diagnostics, Prognosis and Therapy Prediction. Int J Mol Sci. 2022 May 11;23(10):5384.

65. Feng Q, Guo P, Kang S, Zhao F. High expression of TAZ/YAP promotes the progression of malignant melanoma and affects the postoperative survival of patients. Die Pharmazie - An International Journal of Pharmaceutical Sciences. 2018 Nov 1;73(11):662–5.

66. Kim MH, Kim J, Hong H, Lee S, Lee J, Jung E, Kim J. Actin remodeling confers BRAF inhibitor resistance to melanoma cells through YAP/TAZ activation. EMBO J. 2016 Mar 1;35(5):462–78.

67. Chakrabarti SK, Kardile H, Tiwari JK. Plant biotechnology: Progress in genomic era. In: Tikhonovich AA, McHughen BRJAED, Tiwari VK, editors. Current Trends in Biotechnology: From Genome Sequence to Crop Improvement. Singapore: Springer; 2019 Nov 15;p. 91–108.

68. Schena M, Heller RA, Theriault TP, Konrad K, Lachenmeier E, Davis RW. Microarrays: biotechnology's discovery platform for functional genomics. Trends in Biotechnology. 1998 Jul 1;16(7):301–6.

69. Fodor SP, Read JL, Pirrung MC, Stryer L, Lu AT, Solas D. Light-directed, spatially addressable parallel chemical synthesis. Science. 1991 Feb 15;251(4995):767–73.

70. Schena M, Shalon D, Davis RW, Brown PO. Quantitative monitoring of gene expression patterns with a complementary DNA microarray. Science. 1995 Oct 20;270(5235):467–70.

71. Heller MJ. DNA Microarray Technology: Devices, Systems, and Applications. Annual Review of Biomedical Engineering. 2002 Aug 1;4(Volume 4, 2002):129–53.

72. Wang Z, Gerstein M, Snyder M. RNA-Seq: a revolutionary tool for transcriptomics. Nat Rev Genet. 2009 Jan;10(1):57–63.

73. Chu Y, Corey DR. RNA Sequencing: Platform Selection, Experimental Design, and Data Interpretation. Nucleic Acid Ther. 2012 Aug;22(4):271–4.

74. Ardui S, Ameur A, Vermeesch JR, Hestand MS. Single molecule real-time (SMRT) sequencing comes of age: applications and utilities for medical diagnostics. Nucleic Acids Res. 2018 Mar 16;46(5):2159–68.

75. Jain M, Olsen HE, Paten B, Akeson M. The Oxford Nanopore MinION: delivery of nanopore sequencing to the genomics community. Genome Biol. 2016;17(1):239.

76. Harrington CT, Lin EI, Olson MT, Eshleman JR. Fundamentals of Pyrosequencing. Archives of Pathology & Laboratory Medicine. 2013 Sep 1;137(9):1296–303.

77. Rothberg JM, Hinz W, Rearick TM, Schultz J, Mileski W, Davey M, Leamon JH, Johnson K, Milgrew MJ, Edwards M, Hoon J, Simons JF, Marran D, Myers JW, Davidson JF, Branting A, Nobile JR, Puc BP, Light D, Clark TA, Huber M, Branciforte JT, Stoner IB, Cawley SE, Lyons M, Fu Y, Homer N, Sedova M, Miao X, Reed B, Sabina J, Feierstein E, Schorn M, Alanjary M, Dimalanta E, Dressman D, Kasinskas R, Sokolsky T, Fidanza JA, Namsaraev E, McKernan KJ, Williams A, Roth GT, Bustillo J. An integrated semiconductor device enabling non-optical genome sequencing. Nature. 2011 Jul;475(7356):348–52.

78. Geiss GK, Bumgarner RE, Birditt B, Dahl T, Dowidar N, Dunaway DL, Fell HP, Ferree S, George RD, Grogan T, James JJ, Maysuria M, Mitton JD, Oliveri P, Osborn JL, Peng T, Ratcliffe AL, Webster PJ, Davidson EH, Hood L, Dimitrov K. Direct

multiplexed measurement of gene expression with color-coded probe pairs. Nat Biotechnol. 2008 Mar;26(3):317–25.

79. Edgar R, Domrachev M, Lash AE. Gene Expression Omnibus: NCBI gene expression and hybridization array data repository. Nucleic Acids Res. 2002 Jan 1;30(1):207–10.

80. Eddy JA, Thorsson V, Lamb AE, Gibbs DL, Heimann C, Yu JX, Chung V, Chae Y, Dang K, Vincent BG, Shmulevich I, Guinney J. CRI iAtlas: an interactive portal for immuno-oncology research. F1000Res. 2020;9:1028.

81. Kovács SA, Kovács T, Lánczky A, Paál Á, Hegedűs ZI, Sayour NV, Szabó L, Kovács A, Bianchini G, Ferdinandy P, Ocana A, Varga ZV, Fekete JT, Győrffy B. Unlocking the power of immune checkpoint inhibitors: Targeting YAP1 reduces anti-PD1 resistance in skin cutaneous melanoma. Br J Pharmacol. 2025 May 5;

82. Wang J, Perry CJ, Meeth K, Thakral D, Damsky W, Micevic G, Kaech S, Blenman K, Bosenberg M. UV-induced somatic mutations elicit a functional T cell response in the YUMMER1.7 Mouse Melanoma Model. Pigment Cell Melanoma Res. 2017 Jul;30(4):428–35.

83. Yu JW, Bhattacharya S, Yanamandra N, Kilian D, Shi H, Yadavilli S, Katlinskaya Y, Kaczynski H, Conner M, Benson W, Hahn A, Seestaller-Wehr L, Bi M, Vitali NJ, Tsvetkov L, Halsey W, Hughes A, Traini C, Zhou H, Jing J, Lee T, Figueroa DJ, Brett S, Hopson CB, Smothers JF, Hoos A, Srinivasan R. Tumor-immune profiling of murine syngeneic tumor models as a framework to guide mechanistic studies and predict therapy response in distinct tumor microenvironments. PLoS One. 2018 Nov 2;13(11):e0206223.

84. Tomayko MM, Reynolds CP. Determination of subcutaneous tumor size in athymic (nude) mice. Cancer Chemother Pharmacol. 1989 Sep 1;24(3):148–54.

85. Chen PL, Roh W, Reuben A, Cooper ZA, Spencer CN, Prieto PA, Miller JP, Bassett RL, Gopalakrishnan V, Wani K, De Macedo MP, Austin-Breneman JL, Jiang H, Chang Q, Reddy SM, Chen WS, Tetzlaff MT, Broaddus RJ, Davies MA,

Gershenwald JE, Haydu L, Lazar AJ, Patel SP, Hwu P, Hwu WJ, Diab A, Glitza IC, Woodman SE, Vence LM, Wistuba II, Amaria RN, Kwong LN, Prieto V, David RE, Ma W, Overwijk WW, Sharpe AH, Hu J, Futreal PA, Blando J, Sharma P, Allison JP, Chin L, Wargo JA. Analysis of Immune Signatures in Longitudinal Tumor Samples Yields Insight into Biomarkers of Response and Mechanisms of Resistance to Immune Checkpoint Blockade. Cancer Discov. 2016 Aug;6(8):827–37.

86. Litchfield K, Reading JL, Puttick C, Thakkar K, Abbosh C, Bentham R, Watkins TBK, Rosenthal R, Biswas D, Rowan A, Lim E, Al Bakir M, Turati V, Guerra-Assunção JA, Conde L, Furness AJS, Saini SK, Hadrup SR, Herrero J, Lee SH, Van Loo P, Enver T, Larkin J, Hellmann MD, Turajlic S, Quezada SA, McGranahan N, Swanton C. Meta-analysis of tumor- and T cell-intrinsic mechanisms of sensitization to checkpoint inhibition. Cell. 2021 Feb 4;184(3):596-614.e14.

87. Kim ST, Cristescu R, Bass AJ, Kim KM, Odegaard JI, Kim K, Liu XQ, Sher X, Jung H, Lee M, Lee S, Park SH, Park JO, Park YS, Lim HY, Lee H, Choi M, Talasaz AA, Kang PS, Cheng J, Loboda A, Lee J, Kang WK. Comprehensive molecular characterization of clinical responses to PD-1 inhibition in metastatic gastric cancer. Nat Med. 2018 Sep;24(9):1449–58.

88. Miao D, Margolis CA, Gao W, Voss MH, Li W, Martini DJ, Norton C, Bossé D, Wankowicz SM, Cullen D, Horak C, Wind-Rotolo M, Tracy A, Giannakis M, Hodi FS, Drake CG, Ball MW, Allaf ME, Snyder A, Hellmann MD, Ho T, Motzer RJ, Signoretti S, Kaelin WG, Choueiri TK, Van Allen EM. Genomic correlates of response to immune checkpoint therapies in clear cell renal cell carcinoma. Science. 2018 Feb 16;359(6377):801–6.

89. Liu D, Schilling B, Liu D, Sucker A, Livingstone E, Jerby-Arnon L, Zimmer L, Gutzmer R, Satzger I, Loquai C, Grabbe S, Vokes N, Margolis CA, Conway J, He MY, Elmarakeby H, Dietlein F, Miao D, Tracy A, Gogas H, Goldinger SM, Utikal J, Blank CU, Rauschenberg R, von Bubnoff D, Krackhardt A, Weide B, Haferkamp S, Kiecker F, Izar B, Garraway L, Regev A, Flaherty K, Paschen A, Van Allen EM, Schadendorf D. Integrative molecular and clinical modeling of clinical outcomes to

PD1 blockade in patients with metastatic melanoma. Nat Med. 2019 Dec;25(12):1916–27.

90. Cristescu R, Mogg R, Ayers M, Albright A, Murphy E, Yearley J, Sher X, Liu XQ, Lu H, Nebozhyn M, Zhang C, Lunceford JK, Joe A, Cheng J, Webber AL, Ibrahin N, Plimack ER, Ott PA, Seiwert TY, Ribas A, McClanahan TK, Tomassini JE, Loboda A, Kaufman D. Pan-tumor genomic biomarkers for PD-1 checkpoint blockade-based immunotherapy. Science. 2018 Oct 12;362(6411):eaar3593.

91. Gide TN, Quek C, Menzies AM, Tasker AT, Shang P, Holst J, Madore J, Lim SY, Velickovic R, Wongchenko M, Yan Y, Lo S, Carlino MS, Guminski A, Saw RPM, Pang A, McGuire HM, Palendira U, Thompson JF, Rizos H, Silva IPD, Batten M, Scolyer RA, Long GV, Wilmott JS. Distinct Immune Cell Populations Define Response to Anti-PD-1 Monotherapy and Anti-PD-1/Anti-CTLA-4 Combined Therapy. Cancer Cell. 2019 Feb 11;35(2):238-255.e6.

92. Mariathasan S, Turley SJ, Nickles D, Castiglioni A, Yuen K, Wang Y, Kadel EE, Koeppen H, Astarita JL, Cubas R, Jhunjhunwala S, Banchereau R, Yang Y, Guan Y, Chalouni C, Ziai J, Şenbabaoğlu Y, Santoro S, Sheinson D, Hung J, Giltname JM, Pierce AK, Mesh K, Lianoglou S, Riegler J, Carano RAD, Eriksson P, Hoglund M, Somarriba L, Halligan DL, van der Heijden M, Loriot Y, Rosenberg JE, Fong L, Mellman I, Chen DS, Green M, Derleth C, Fine GD, Hegde PS, Bourgon R, Powles T. TGF-β attenuates tumour response to PD-L1 blockade by contributing to exclusion of T cells. Nature. 2018 Feb 22;554(7693):544–8.

93. Van Allen EM, Miao D, Schilling B, Shukla SA, Blank C, Zimmer L, Sucker A, Hillen U, Foppen MHG, Goldinger SM, Utikal J, Hassel JC, Weide B, Kaehler KC, Loquai, C, Mohr P, Gutzmer R, Dummer R, Gabriel S, Wu CJ, Schadendorf D, Garraway LA. Genomic correlates of response to CTLA-4 blockade in metastatic melanoma. Science. 2015 Oct 9;350(6257):207–11.

94. Lamar JM, Xiao Y, Norton E, Jiang ZG, Gerhard GM, Kooner S, Warren JSA, Hynes RO. SRC tyrosine kinase activates the YAP/TAZ axis and thereby drives tumor growth and metastasis. J Biol Chem. 2019 Feb 15;294(7):2302–17.

95. Vassilev A, Kaneko KJ, Shu H, Zhao Y, DePamphilis ML. TEAD/TEF transcription factors utilize the activation domain of YAP65, a Src/Yes-associated protein localized in the cytoplasm. Genes Dev. 2001 May 15;15(10):1229–41.

96. Oudhoff MJ, Braam MJS, Freeman SA, Wong D, Rattray DG, Wang J, Antignano F, Snyder K, Refaeli I, Hughes MR, McNagny KM, Gold MR, Arrowsmith CH, Sato T, Rossi FMV, Tatlock JH, Owen DR, Brown PJ, Zaph C. SETD7 Controls Intestinal Regeneration and Tumorigenesis by Regulating Wnt/β-Catenin and Hippo/YAP Signaling. Dev Cell. 2016 Apr 4;37(1):47–57.

97. Jin L, Chen Y, Cheng D, He Z, Shi X, Du B, Xi X, Gao Y, Guo Y. YAP inhibits autophagy and promotes progression of colorectal cancer via upregulating Bcl-2 expression. Cell Death Dis. 2021 May 7;12(5):1–10.

98. Yang H, Zhu J, Wang G, Liu H, Zhou Y, Qian J. STK35 Is Ubiquitinated by NEDD4L and Promotes Glycolysis and Inhibits Apoptosis Through Regulating the AKT Signaling Pathway, Influencing Chemoresistance of Colorectal Cancer. Front Cell Dev Biol. 2020;8:582695.

99. Wong CH, Siah KW, Lo AW. Estimation of clinical trial success rates and related parameters. Biostatistics. 2019 Apr 1;20(2):273–86.

100. Moreira JMA, Ohlsson G, Gromov P, Simon R, Sauter G, Celis JE, Gromova I. Bladder cancer-associated protein, a potential prognostic biomarker in human bladder cancer. Mol Cell Proteomics. 2010;9(1):161–77.

101. Huang YT, Wu TS, Lu CC, Yu FY, Liu BH. Aristolochic acid I interferes with the expression of BLCAP tumor suppressor gene in human cells. Toxicol Lett. 2018 Jul;291:129–37.

102. Sweis RF, Spranger S, Bao R, Paner GP, Stadler WM, Steinberg G, Gajewski TF. Molecular Drivers of the Non-T-cell-Inflamed Tumor Microenvironment in Urothelial Bladder Cancer. Cancer Immunol Res. 2016 Jul;4(7):563–8.

103. Chen S, Zhang N, Shao J, Wang T, Wang X. Multi-omics Perspective on the Tumor Microenvironment based on PD-L1 and CD8 T-Cell Infiltration in Urothelial Cancer. J Cancer. 2019 Jan 1;10(3):697–707.

104. Palakurthi S, Kuraguchi M, Zacharek SJ, Zudaire E, Huang W, Bonal DM, Liu J, Dhaneshwar A, DePeaux K, Gowaski MR, Bailey D, Regan SN, Ivanova E, Ferrante C, English JM, Khosla A, Beck AH, Rytlewski JA, Sanders C, Laquerre S, Bittinger MA, Kirschmeier PT, Packman K, Janne PA, Moy C, Wong KK, Verona RI, Lorenzi MV. The Combined Effect of FGFR Inhibition and PD-1 Blockade Promotes Tumor-Intrinsic Induction of Antitumor Immunity. Cancer Immunol Res. 2019 Sep;7(9):1457–71.

105. Kommalapati A, Tella SH, Borad M, Javle M, Mahipal A. FGFR Inhibitors in Oncology: Insight on the Management of Toxicities in Clinical Practice. Cancers (Basel). 2021 Jun 13;13(12):2968.

106. Zengin ZB, Chehrazi-Raffle A, Salgia NJ, Muddasani R, Ali S, Meza L, Pal SK. Targeted therapies: Expanding the role of FGFR3 inhibition in urothelial carcinoma. Urologic Oncology: Seminars and Original Investigations. 2022 Feb 1;40(2):25–36.

107. Liu ST, Pham H, Pandol SJ, Ptasznik A. Src as the link between inflammation and cancer. Front Physiol. 2014 Jan 16;4:416.

108. Roberts AW, Wei AH, Huang DCS. BCL2 and MCL1 inhibitors for hematologic malignancies. Blood. 2021 Sep 30;138(13):1120–36.

109. Vogler M. Targeting BCL2-Proteins for the Treatment of Solid Tumours. Adv Med. 2014;2014:943648.

110. Barsyte-Lovejoy D, Li F, Oudhoff MJ, Tatlock JH, Dong A, Zeng H, Wu H, Freeman SA, Schapira M, Senisterra GA, Kuznetsova E, Marcellus R, Allali-Hassani A, Kennedy S, Lamber JP, Couzens AL, Aman A, Gingras AC, Al-Awar R, Fish PV, Gerstenberger BS, Roberts L, Benn CL, Grimley RL, Braam MJS, Rossi FMV, Sudol M, Brown PJ, Bunnage ME, Owen DR, Zaph C, Vedadi M, Arrowsmith CH. (R)-

PFI-2 is a potent and selective inhibitor of SETD7 methyltransferase activity in cells. Proc Natl Acad Sci U S A. 2014 Sep 2;111(35):12853–8.

111. Meng F, Cheng S, Ding H, Liu S, Liu Y, Zhu K, Chen S, Lu J, Xie Y, Li J, Liu R, Shi Z, Zhou Y, Liu YC Zheng M, Jiang H, Lu W, Liu H, Luo C. Discovery and Optimization of Novel, Selective Histone Methyltransferase SET7 Inhibitors by Pharmacophore- and Docking-Based Virtual Screening. J Med Chem. 2015 Oct 22;58(20):8166–81.

112. Ding H, Lu WC, Hu JC, Liu YC, Zhang CH, Lian FL, Zhang NX, Meng FW, Luo C, Chen KX. Identification and Characterizations of Novel, Selective Histone Methyltransferase SET7 Inhibitors by Scaffold Hopping- and 2D-Molecular Fingerprint-Based Similarity Search. Molecules. 2018 Mar 2;23(3):E567.

113. Takemoto Y, Ito A, Niwa H, Okamura M, Fujiwara T, Hirano T, Handa N, Umehara T, Sonoda T, Ogawa K, Tariq M, Nishino N, Dan S, Kagechika H, Yamori T, Yokoyama S, Yoshida M. Identification of Cyproheptadine as an Inhibitor of SET Domain Containing Lysine Methyltransferase 7/9 (Set7/9) That Regulates Estrogen-Dependent Transcription. J Med Chem. 2016 Apr 28;59(8):3650–60.

114. Li D, Guo J, Jia R. Histone code reader SPIN1 is a promising target of cancer therapy. Biochimie. 2021 Dec 1;191:78–86.

115. Oudhoff MJ, Freeman SA, Couzens AL, Antignano F, Kuznetsova E, Min PH, Northrop JP, Lehnertz B, Barsyte-Lovejoy D, Vedadi M, Arrowsmith CH, Nishina H, Gold MR, Rossi FMV, Gingras AC, Zaph C. Control of the hippo pathway by Set7-dependent methylation of Yap. Dev Cell. 2013 Jul 29;26(2):188–94.

116. Lu M, Wang K, Ji W, Yu Y, Li Z, Xia W, Lu S. FGFR1 promotes tumor immune evasion via YAP-mediated PD-L1 expression upregulation in lung squamous cell carcinoma. Cellular Immunology. 2022 Sep 1;379:104577.

117. Ryu HJ, Kim C, Jang H, Kim SI, Shin SJ, Chung KY, Torres-Cabala C, Kim SK. Nuclear Localization of Yes-Associated Protein Is Associated With Tumor Progression in Cutaneous Melanoma. Lab Invest. 2024 May;104(5):102048.

118. Meeth K, Wang J, Micevic G, Damsky W, Bosenberg MW. The YUMM lines: a series of congenic mouse melanoma cell lines with defined genetic alterations. Pigment Cell Melanoma Res. 2016 Sep;29(5):590–7.

119. Castle JC, Kreiter S, Diekmann J, Löwer M, Van de Roemer N, de Graaf J, Selmi A, Diken M, Boegel S, Paret C, Koslowski M, Kuhn AN, Britten CM, Huber C, Türeci Ö, Sahin U. Exploiting the mutanome for tumor vaccination. Cancer Res. 2012 March 1;72(5):1081–1091.

120. Shibata M, Ham K, Hoque MO. A time for YAP1: Tumorigenesis, immunosuppression and targeted therapy. Int J Cancer. 2018;143(9):2133–44.

121. Cunningham R, Hansen CG. The Hippo pathway in cancer: YAP/TAZ and TEAD as therapeutic targets in cancer. Clin Sci. 2022 Feb 11;136(3):197–222.

122. Miskolczi Zs, Smith MP, Rowling EJ, Ferguson J, Barriuso J, Wellbrock C. Collagen abundance controls melanoma phenotypes through lineage-specific microenvironment sensing. Oncogene. 2018 March 16;37(23):3166–3182.

123. Qin SS, Han BJ, Williams A, Jackson KM, Jewell R, Chacon AC, Lord EM, Linehan DC, Kim M, Reuben A, Gerber SA, Prieto PA. Intertumoral Genetic Heterogeneity Generates Distinct Tumor Microenvironments in a Novel Murine Synchronous Melanoma Model. Cancers (Basel). 2021 May 11;13(10):2293.

124. Ladányi A, Rásó E, Barbai T, Vízkeleti L, Puskás LG, Kovács SA, Győrffy B, Tímár J. Identification of a Tumor Cell Associated Type I IFN Resistance Gene Expression Signature of Human Melanoma, the Components of Which Have a Predictive Potential for Immunotherapy. Int J Mol Sci. 2022 Jan;23(5):2704.

125. Vízkeleti L, Papp O, Doma V, Gil J, Markó-Varga G, Kovács SA, Győrffy B, Kárpáti S, Tímár J. Identification of genetic fingerprint of type I interferon therapy in visceral metastases of melanoma. Sci Rep. 2024 Nov 3;14(1):26540.

126. Yu M, Peng Z, Qin M, Liu Y, Wang J, Zhang C, Lin J, Dong T, Wang L, Li S, Yang Y, Xu S, Guo W, Zhang X, Shi M, Peng H, Luo X, Zhang H, Zhang L, Li Y,

Yang XP, Sun S. Interferon-γ induces tumor resistance to anti-PD-1 immunotherapy by promoting YAP phase separation. Mol Cell. 2021 Mar 18;81(6):1216-1230.e9.

127. Ayers M, Lunceford J, Nebozhyn M, Murphy E, Loboda A, Kaufman DR, Albright A, Cheng JD, Kang SP, Shankaran V, Piha-Paul SA, Yearley J, Seiwert TY, Ribas A, McClanahan TK. IFN-γ-related mRNA profile predicts clinical response to PD-1 blockade. J Clin Invest. 2017;127(8):2930–40.

9. BIBLIOGRAPHY OF THE CANDIDATE'S PUBLICATIONS

9.1. Publications related to this dissertation

Kovács, S. A., Kovács, T., Lánczky, A., Paál, Á., Hegedűs, Z. I., Sayour N. V., Szabó, L., Kovács, A., Bianchini, G., Ferdinandy, P., Ocana, A., Varga Z. V., Fekete, J. T., Győrffy, B. Unlocking the power of immune checkpoint inhibitors: Targeting YAP1 reduces anti-PD1 resistance in skin cutaneous melanoma. British Journal of Pharmacology 1-20 (2025). https://doi.org/10.1111/bph.70052

Kovács, S. A., Fekete, J. T. & Győrffy, B. Predictive biomarkers of immunotherapy response with pharmacological applications in solid tumors. Acta Pharmacologica Sinica 44, 1879–1889 (2023). https://doi.org/10.1038/s41401-023-01079-6

Kovács, S. A., Győrffy, B. Transcriptomic datasets of cancer patients treated with immune-checkpoint inhibitors: a systematic review. Journal of Translational Medicine 20, 249 (2022). https://doi.org/10.1186/s12967-022-03409-4

Ladányi, A., Rásó, E., Barbai, T., Vízkeleti, L., Puskás, L. G., **Kovács, S. A**., Győrffy, B., & Tímár, J. Identification of a Tumor Cell Associated Type I IFN Resistance Gene Expression Signature of Human Melanoma, the Components of Which Have a Predictive Potential for Immunotherapy. International Journal of Molecular Sciences, 23(5), 2704 (2022). https://doi.org/10.3390/ijms23052704

9.2. Publications not included in the dissertation

Vízkeleti, L., Papp, O., Doma, V., Gil, J., Markó-Varga, G., **Kovács, S. A**., Győrffy, B., Kárpáti, S., & Tímár, J. Identification of genetic fingerprint of type I interferon therapy in visceral metastases of melanoma. Scientific Reports, 14(1), 26540 (2024). https://doi.org/10.1038/s41598-024-77285-x

10. ACKNOWLEDGEMENTS

I would like to express my deepest gratitude to my supervisor, Prof. Dr. Balázs Győrffy, for his invaluable guidance, expertise, and continuous support throughout my doctoral journey. His dedication to both my research and personal development has been instrumental in shaping my academic growth. I am especially grateful for his prompt responses, insightful advice, and unwavering encouragement, which have made this journey both enriching and fulfilling.

I extend my sincere thanks to all the past and present members of the Department of Bioinformatics, whose support has played a crucial role in helping me navigate the challenges of my PhD years. I would like to give special recognition to Dr. János Tibor Fekete for his statistical guidance in my projects, and Dr. Gyöngyi Munkácsy for her helpful suggestions and assistance. My heartfelt appreciation also goes to my fellow PhD colleagues, Ankita Murmu, Dr. Áron Bartha, Dalma Müller, and, for their unwavering support throughout this endeavor.

I am also profoundly grateful to my scientific collaborators at the Department of Pharmacology and Pharmacotherapy, and the Department of Dermatology, Venereology, and Dermatooncology. In particular, I would like to thank, Dr. Ágnes Paál, Dr. Beáta Kun, Dr. László Horváth, Dr. Zoltán Varga, Tamás Kovács, and Zsombor Hegedűs, whose expertise and contributions were indispensable to my research.

Last but not least, I would like to express my heartfelt gratitude to my family and friends for their constant encouragement, patience, and understanding. Their continuous support and belief in me have been the foundation that sustained me through the challenges and triumphs of this PhD journey.